A comparison between Envisat and ICESat sea ice thickness in the Southern Ocean

Jinfei Wang[1], Chao Min[1], Robert Ricker[2], Qian Shi[1], Bo Han[1], Stefan Hendricks[2], Renhao Wu[1], Qinghua Yang[1]

5   [1]School of Atmospheric Sciences, Sun Yat-sen University, and Southern Marine Science and Engineering Guangdong Laboratory (Zhuhai), Zhuhai 519082, China
[2]Alfred Wegener Institute Helmholtz Centre for Polar and Marine Research, Bremerhaven 27570, Germany

Correspondence to: Qian Shi (shiq9@mail.sysu.edu.cn)

Abstract. The crucial role that Antarctic sea ice plays in the global climate system is strongly linked to its thickness. While
10   field observations are too sparse in the Southern Ocean to determine long-term trends of the Antarctic sea ice thickness (SIT) on a hemispheric scale, satellite radar altimetry data can be applied with a promising prospect. European Space Agency Climate Change Initiative – Sea Ice Project (ESA SICCI) generates sea ice thickness derived from Envisat, covering the entire Southern Ocean year-round from 2002 to 2012. In this study, the SICCI Envisat Antarctic SIT is first compared with an ICESat SIT product retrieved with a modified ice density algorithm. Both data sets are compared to SIT estimates from upward−looking
15   sonar (ULS) in the Weddell Sea, showing mean differences (MD) and standard deviations (SD) of 1.29 (0.65) m for Envisat-ULS (- denotes 'minus' and same as below), while we find 1.11 (0.81) m for ICESat-ULS, respectively. The inter-comparisons are conducted for three seasons except for winter, based on the ICESat operating periods. According to the results, the differences between Envisat and ICESat SIT reveal significant temporal and spatial variations. More specifically, the smallest seasonal SIT MD (SD) of 0.00 m (0.39 m) for Envisat-ICESat is found in spring (October-November), while larger MD (SD)
20   of 0.52 m (0.68 m) and 0.57 m (0.45 m) exist in summer (February-March) and autumn (May-June). It is also shown that from autumn to spring, mean Envisat SIT decreases while mean ICESat SIT increases. Our findings suggest that both overestimation of Envisat sea ice freeboard potentially caused by radar backscatter originating from inside the snow layer, as well as the AMSR-E snow depth biases and sea ice density uncertainties can possibly account for the differences between Envisat and ICESat SIT.

25   # 1 Introduction

Antarctic sea ice plays an important role in the global climate system by reflecting the solar energy and modulating the surface water salinity (Goosse and Zunz, 2014; Massom et al., 2018; Maksym, 2019). In the context of global warming and the significant decline of Arctic sea ice cover, the Antarctic sea ice area has unexpectedly increased over recent decades (Zhang, 2007; Parkinson and Cavalieri, 2012; Comiso et al., 2017), but dropped to a historic low in 2017 (Turner and Comiso, 2017).

30   During 2016-2020, the sea ice coverage in the Southern Ocean did not recover and set eight new Antarctic monthly record lows instead (Parkinson and DiGirolamo, 2021). However, it is still unclear if the recent increase in the Antarctic sea ice area is also accompanied by a similar change in sea ice thickness. Sea ice thickness combined with sea ice area is necessary to quantify the sea ice volume and sea ice mass (e.g., Kurtz and Markus, 2012; Massonnet et al., 2013). Changes in sea ice volume can influence the fresh water input into the Southern Ocean. Moreover, sea ice thickness is also necessary for assessing

35   sea ice mass balance and surface energy budget, and predicting changes in the polar climate system. Compared to the Arctic, knowledge about Antarctic sea ice thickness is still sparse. More accurate estimations are needed to monitor and quantify global sea ice volume more precisely (Connor et al., 2009), and improve sea ice components in model simulations (e.g., McLaren et al., 2006).

    However, Antarctic sea ice thickness information is difficult to obtain. One type of observation data is in-situ measurements

40   providing sea ice thickness at fixed locations and some allowing to check the consistency over time. For example, drilling data (e.g., Meiners et al., 2012) are accurate but extremely limited in temporal and spatial coverage, and hence they cannot be used to understand large-scale Antarctic sea ice thickness distributions. Upward-looking sonars (ULS), located at 13 different sites in the Weddell Sea, provide valuable temporal evolutions of sea ice draft (Harms et al., 2001; Behrendt et al., 2013a; Behrendt et al., 2013b), but a basin-wide spatial distribution cannot be derived. The other type of data set has short durations but high

45   resolutions, covering comparably large regions and hence allowing to check the spatial variability of the sea ice thickness retrieved from satellite data. Ship-based observations collected by the Antarctic Sea Ice Processes and Climate (ASPeCt) expert group (Worby et al., 2008a) can provide more spatial information than drilling, but they tend to underestimate the actual thickness because of visual interpretation limitations and biases due to ship routing preferably through thinner ice (Giles et al., 2008; Williams et al., 2015). In addition, airborne electromagnetic (AEM) data which provide total freeboard (sea ice freeboard

50   plus snow depth) were collected during expeditions like ISPOL (2004/05) (El Naggar et al., 2007), WWOS (2006) (Lemke, 2009) and AWECS (2013) (Lemke, 2014). Yet, the Antarctic AEM data are still sparse and have mostly been obtained in the Weddell Sea. The airborne remote sensing program NASA Operation IceBridge provides along-track data of total freeboard and snow depth estimations in the Weddell Sea and Amundsen-Bellingshausen Sea (Koenig et al., 2010), which have been investigated in some valuable studies previously (e.g., Kwok and Maksym, 2014; Kwok and Kacimi, 2018; Wang et al., 2020).

55   Despite covering limited regions and/or time periods, all these various observational data sets are extremely useful for the evaluation of models and satellite retrieval methods. More recently, satellite remote sensing has been widely applied to investigate the spatial coverage and long-term trends of sea ice thickness over the whole Southern Ocean. Passive microwave sensors are used to obtain thin ice thickness (below 20 cm) by retrieving the brightness temperature, and are effectively applied in coastal polynyas (Nihashi and Ohshima, 2015). Satellite altimetry, including radar and laser altimetry, has also been used

60   to retrieve sea ice thickness (e.g., Giles et al., 2008; Kurtz and Markus, 2012; Kacimi and Kwok, 2020) and has proven to currently be the best source for Antarctic-wide sea ice thickness retrieval over the full thickness range.

Within the framework of the Sea Ice Climate Change Initiative (SICCI) project, radar altimeter data collected by European Space Agency (ESA) satellites over the past two decades have been reprocessed and assessed. Based on these data, a new SICCI sea ice thickness data set was released in 2018 as version 2.0, including the two radar altimetry satellites, Envisat and

65 CryoSat-2 (Hendricks et al., 2018a; Hendricks et al., 2018b). The SICCI product covers the entire Antarctic sea ice for the complete annual cycle from 2002 to 2017. SIT retrieval from radar altimetry is based on the assumption that the dominant source of radar backscatter is the snow/ice interface (Beaven et al., 1995) and sea ice freeboard is measured by differential ranging over sea ice and ocean surfaces, illustrated in Fig. 1. Snow affects the radar altimetry SIT retrieval in two ways. Firstly, snow depth is required to correct the radar wave speed in snow and hence to appropriately convert the radar freeboard into the

70 sea ice freeboard, as well as to convert sea ice freeboard into sea ice thickness. Secondly, the presence of snow modifies how the radar signal is reflected by the ice-snow system. Specifically, over Antarctic sea ice, the complex snow stratigraphy and frequent snow flooding associated with the formation of snow ice and superimposed ice affect radar altimetry measurements (Willatt et al., 2010), i.e., the assumption of Beaven et al. (1995) is for DRY snow only. Besides, the snow depth climatology used in the retrieval of Envisat and CryoSat-2 SIT can cause biases due to neglecting inter-annual variability in snow depth

75 (Bunzel et al., 2018). The SICCI Antarctic SIT data record has therefore been categorized as experimental data by the data producers compared to a more mature climate data record in the Arctic. Additional uncertainties of the radar altimeter range retrieval arise from the surface type mixing (Schwegmann et al., 2016; Paul et al., 2018; Tilling et al., 2019) and surface roughness (Hendricks et al., 2010; Ricker et al., 2014; Landy et al., 2020). Due to larger footprints compared with laser altimeters, radar altimeter measurements can be more affected by surface type mixing and surface roughness.

80 The Geoscience Laser Altimeter System (GLAS) aboard the Ice, Cloud and land Elevation Satellite (ICESat) allows estimating the total freeboard through the determination of the surface elevation from 2003 to 2009, illustrated in Fig. 1. This dataset has been used in previous studies for many years (e.g., Markus et al., 2011; Yi et al., 2011; Kurtz and Markus, 2012; Xie et al., 2013; Kern and Spreen, 2015). In contrast to radar altimetry, laser altimetry has the advantage of a well-defined reflective horizon, which is the air/snow interface. The main deficiencies of ICESat data are data gaps due to cloud coverage, and more

85 generally the discontinuous and short observation periods. Therefore, ICESat data cannot reflect the current characteristics of the fast-changing Antarctic sea ice. However, ICESat-2, which has been in orbit since 2018, provides a new source of year-round observations of total freeboard and better coverage than ICESat (Kwok et al., 2019; Kacimi and Kwok, 2020).

Both the Envisat and CryoSat-2 SIT in the Southern Ocean have already been evaluated with the drilling data, AEM, ULS and ship-based data (Kern et al., 2018). These evaluations are comprehensive but still have their limitations due to small spatial

90 coverage or short temporal coverage. Thus, we cannot achieve an overall understanding of their data quality. To get a better understanding of the characteristics of the SICCI product version 2.0, we aim to investigate how the SICCI Envisat SIT compares with the ICESat SIT, also how the different altimeters and retrieval methods are represented in the SIT distribution. Based on the former inter-comparison study (Kern et al., 2016), we choose the ICESat SIT derived from the modified density

approach for comparison, which seems to agree with average SIT from independent observations like ASPeCt, ULS and AEM

95 and has a reasonable winter-to-spring growth (Kern et al., 2016). Furthermore, in order to evaluate the ICESat and Envisat data in the Weddell Sea, we also compare both SIT records with the Weddell Sea ULS data first.

The study is organized as follows. In section 2, we describe the data used in this study in detail. Section 3 presents the results of both the Weddell Sea ULS data validations and the inter-comparisons between the two satellite data sets. Potential reasons for the spatial and temporal differences are discussed in section 4. The main results are summarized in section 5.

100 **2 Data and methods**

2.1 Sea ice thickness from Envisat / RA-2

SICCI provides a set of Antarctic sea ice freeboard and thickness data (Hendricks et al., 2018b) obtained from the satellite missions Envisat (2002–2012) and CryoSat-2 (2010–2017). With 50-km grid resolution and monthly temporal resolution, there is a successive year-round record for Antarctic sea ice freeboard and thickness on Equal-Area Scalable Earth (EASE) grid.

105 Since only Envisat shares overlapping periods with ICESat, we focus on the characteristics of the Envisat radar altimeter. Envisat was launched on 01 March 2002 and the mission ended on 08 April 2012. The Radar Altimeter 2 (RA-2) aboard Envisat is a nadir-looking pulse limited sensor operating at the main frequency of 13.575 GHz (Ku-Band), with a secondary frequency of 3.2 GHz (S-Band) compensating the ionospheric error (Zelli and Aerospazio, 1999). It has an orbit inclination of 98.55°, covering the whole ice-covered Southern Ocean and nominal circular footprints of 2–10 km in diameter (Peacock and

110 Laxon, 2004; Connor et al., 2009). Because the RA-2 is the only altimeter carried by Envisat, we refer to it as Envisat hereafter.

The Envisat radar freeboard is retrieved based on the radar ranges obtained from RA-2 Level-1 waveform data over ice surface and leads between ice floes. Ideally, the signal will return at the interface between snow and ice based on the experience from laboratory work (Beaven et al., 1995). Then, snow-depth dependent radar signal delay is applied to convert the radar freeboard into the sea ice freeboard. The illustration of sea ice freeboard is shown in Fig. 1, which is the sea ice surface elevation relative

115 to the sea surface elevation. Sea ice thickness is retrieved from sea ice freeboard based on the hydrostatic equilibrium approach as first used by Laxon et al. (2003), who apply this method on ERS altimetry, which is the predecessor of the Envisat RA-2 instrument:

$$I = \frac{F\rho_{water} + S\rho_{snow}}{\rho_{water} - \rho_{ice}} \tag{1}$$

where F represents Envisat sea ice freeboard, S represents snow depth, I represents sea ice thickness, ρ_{water}, ρ_{snow}, ρ_{ice} refer

120 to the densities of the sea water, snow and sea ice, respectively. A snow depth climatology is employed to retrieve sea ice thickness from sea ice freeboard here (Markus and Cavalieri, 1998; Comiso et al., 2003). This snow depth climatology is

derived from the passive microwave sensor Advanced Microwave Scanning Radiometer-EOS/2 (AMSR-E, 2002-2011; AMSR2, 2012-2017) and is based on a revised approach with different tie point retrieval plus addition of retrieval errors and provided by the Integrated Climate Data Center (ICDC).

125   In addition, it is noted that Envisat sea ice thickness represents the actual SIT (i.e., SIT of the ice-covered fraction of the grid cell area) and values with sea ice concentration (SIC) less than 70 % have been removed during Envisat SIT retrieval.

2.2 Sea ice thickness from ICESat / GLAS

ICESat, operating as part of NASA's Earth Observing System, provides a set of Antarctic total freeboard from 2003 to 2009. Different from the sea ice freeboard measured by radar altimeters, laser altimeters allow to detect the distance between the
130   snow surface and sea surface, as shown in Fig. 1. ICESat measurements are characterized by laser footprints of ~70 m and sampling distances of 170 m (Kwok et al., 2004). However, the measurements are not continuous due to cloud coverage and each measurement campaign lasted for about 35 days (see Fig. 3 in Kern and Spreen, 2015). There are several ICESat SIT data sets derived from different retrieval algorithms. Qualitative inter-comparisons have been done among several ICESat freeboard-to-thickness retrieval approaches (Kern et al., 2016). According to their conclusions, we choose the product derived
135   with the modified density approach in this study, because of its reasonable winter-to-spring increase and better agreements with independent data. The data set is provided by ICDC on the polar-stereographic grid. The approach considers the snow–ice layer as one system with a modified density, in order to avoid using a potentially biased snow depth product. According to Kern et al. (2016), the modified density can be derived as follows:

$$\rho_{ice}^* = \frac{R\rho_{ice} + \rho_{snow}}{R + 1} \tag{2}$$

140   where R is the ratio of sea ice thickness over snow depth, which is a seasonally dependent factor and calculated from ASPeCt observations (Worby et al., 2008a). And total thickness (sea ice thickness plus snow depth) can be determined from it:

$$I = F \frac{\rho_{water}}{\rho_{water} - \rho_{ice}^*} \tag{3}$$

where F represents ICESat total freeboard. Although this method cannot obtain the real SIT, it still extracts the SIT information to a large extent. Meanwhile, we will discuss the biases caused by this method in Sect. 4.

145   The Antarctic mean gridded total freeboard and effective sea ice thickness (i.e., mean thickness per grid cell including open water areas) with a grid resolution of 100 km from 2004 to 2008 are provided in this product. Table 1 presents the available time periods of this data set. It is noted that grid cells with SIC less than 60 % have been removed for the ICESat SIT retrieval.

2.3 Sea ice thickness from Weddell Sea ULS

The upward-looking sonars (ULS) located in the Weddell Sea provide long-term and high-frequency sea ice draft at each site (Behrendt et al., 2013a; Behrendt et al., 2013b). The sensors transmit sound pulses upwards with a footprint of 6–8 m in diameter and the signals are reflected either by the sea ice bottom or the sea surface, yielding two-way travel time which can be converted into distances. The sea ice draft, which is the depth of the sea ice underwater, can consequently be derived from the difference of the two distances, shown in Fig.1. The intervals of sea ice draft measurements are between 3 and 15 minutes from November 1990 to March 2008. In this study, we use the monthly average sea ice draft from 2004 to 2008 at three sites, corresponding to Envisat and ICESat operating time. According to Behrendt (2013), the uncertainties of sea ice draft vary from 5 cm to 12 cm, depending on the seasons. The uncertainty in summer is smaller than in other seasons because open water occurs more frequently in the ULS footprint and thus the estimate of the sea surface height is more accurate. The mooring locations used in this study are shown in Fig. 2. Sea ice thickness (z) is converted from the sea ice draft (d) through an empirical formula established from drilling data in the Weddell Sea (Harms et al., 2001):

$$z \text{ (m)} = 0.028 + 1.012d \text{ (m)}. \tag{4}$$

This empirical equation is based on the assumption that the snow depth values from drillings and ULS are comparable. But it still bears the uncertainties from the production of slush and snow ice caused by flooding (Harms et al., 2001). All the SIT data used in this study have been summarized in Table 2.2.5 Spatial and seasonal divisions.

The comparisons are done for different seasons and different sectors between the two SIT data sets. The seasonal classification is based on the ICESat operating periods presented in Table 1 following Kurtz and Markus (2012). For each ICESat operating period, we choose the corresponding Envisat monthly data, also given in Table 1. We employ a time-weighted average of the monthly Envisat data to match the ICESat period. For example, considering the ON04 period from Oct 3 to Nov 8 in 2004, which is 37 days long – 29 days in October and 8 days in November, we calculate the corresponding Envisat SIT as: SIT_{ON04} = (29/37)*($SIT_{October}$) + (8/37)*($SIT_{November}$). We use this weighing equation only for grid cells where valid Envisat SIT data exist in both months, while the weighing is not conducted for grid cells where valid data only exist in either one month. It is noted that this approach can lead to considerably larger coverage of Envisat SIT data than ICESat, thus we only show grid cells where both Envisat and ICESat have valid SIT and only take those values in the statistical computation.

Besides, Antarctic sea ice characteristics differ remarkably in different areas in the Southern Ocean. Therefore, we divide it into six sectors (Fig. 2) following Worby et al. (2008a) and discuss the differences for each of them.

3 Results and discussion

3.1 Comparisons with Weddell Sea ULS

Before the inter-comparison between Envisat and ICESat SIT, both of them are compared with ULS observations. The ULS sea ice draft has been converted into monthly sea ice thickness data with Eq. (4) in Sect. 2.3. Both Envisat and ICESat SIT have been interpolated onto each ULS location in the nearest neighbour way. In order to compare the SIT from the two satellites with the ULS observations, we first compute the ICESat effective SIT by dividing the SIT by the SIC at each grid cell. The SIC data are derived from Special Sensor Microwave/Imager (SSM/I) and Special Sensor Microwave/Imager Sounder (SSM/IS) based on ASI algorithm provided by ICDC (Kaleschke et al., 2001; https://www.cen.uni-hamburg.de/en/icdc/data/cryosphere/seaiceconcentration-asi-ssmi.html) with 12.5 km spatial resolution, interpolated to 100 km grid NSIDC polar-stereographic grid and averaged over respective ICESat measurement periods. During ICESat operating periods, there are only three sites with valid data for the comparison: 207, 229 and 231 (shown in Fig. 2). The sites can be divided into two regions. Site 207 is near the coast of the Antarctic Peninsula, mostly characterized by perennial ice, while the others belong to the eastern Weddell Sea, predominantly characterized by first-year ice. The corresponding time periods of each SIT product are listed in Table 3.

Figure 3 presents the time series of sea ice thickness for Weddell Sea ULS, Envisat and ICESat at each site. Due to the operating period gaps and lack of valid data along the coast, ICESat only provides a limited number of measurements for comparison. The gaps of Envisat SIT originate from grid cells with SIC below 70%, or missing data caused by failure of retrieval or instrument. The error bars show the uncertainty estimates from the SIT products. Envisat SIT uncertainties are computed as the error propagation of all input uncertainties with the assumption that the sea water density is negligible (see Section 2.9.8 in Paul et al., 2017). ICESat SIT uncertainties are also calculated based on the uncertainties of densities and freeboard (Kern et al., 2016). We also add the ULS error bars by calculating SDs of the ULS SIT for each month. We find that either Envisat or ICESat SIT is not consistent with the sea ice thickness observed from ULS. In the western Weddell Sea along the coast of the Antarctic Peninsula (at site 207), the ULS thickness ranges between 0 and 1.5 m, without a clear seasonal cycle due to a mixture of deformed and undeformed sea ice (Williams et al., 2015). Envisat thickness exceeds ULS, with a maximum value larger than 5 m. In comparison, ICESat thickness also exceeds ULS and only few ULS observations fall within the possible ICESat SIT range indicated by the error bars. In the eastern Weddell Sea (at sites 229 and 231), ICESat has a few overestimations while Envisat has larger overestimations. Noted that the realistic ICESat SIT would be considerably smaller due to the retrieval method mentioned in Sect. 2.2, about 0.2–0.4 m at site 207 and 0.15–0.3 m at site 229/231 depending on the seasons (Fig. S3). The differences in the error bars between Envisat and ICESat mainly result from their different spatial scales, the inclusion of snow depth uncertainty and lack of adequate regards for potential correlations between the error contribution in Envisat SIT, hence making it difficult to estimate realistic uncertainties. Table 4 shows the MDs, SDs, root mean square deviations (RMSDs) for Envisat-ULS and ICESat-ULS, and the numbers of comparison pairs. The Envisat and

ULS SIT are all time-weighted processed and the calculations are conducted when all three products have valid data. The statistics show that both MDs are the largest at site 207 (1.63 m for Envisat-ULS and 1.73 m for ICESat-ULS) and the smallest at site 229 (0.72 m for Envisat-ULS and 0.42 m for ICESat-ULS). However, the numbers of valid data are too small to derive a reliable conclusion on the accuracy of ICESat. The comparison is based on more data pairs for Envisat, but the agreement of the seasonal cycle is bad qualitatively (Fig. 3).

The uncertainties of such comparisons cannot be ignored. The ULS measurements are recorded at fixed locations with approximately 6–8 m footprint in diameter, while Envisat (ICESat) has a footprint of 2–10 km (70 m) and the SIT data used in the comparison represent mean values over 50 km (100 km) grid cells. Large resolution differences can increase the selection biases. When the ULS measures a single point like a ridge or the edge of thin ice, satellites will survey a large area. In addition, though the ULS SIT and satellite SIT are all monthly mean values, one ICESat SIT grid cell is scanned once or twice on most occasions through a measurement period (see Fig. 3 in Kern and Spreen, 2015). Averages based on such a small number of measurements have a limited representation of the mean SIT throughout the whole month. Theoretically, the more valid measurements exist in one grid cell, the more accurate the mean SIT is. In general, uncertainties from both spatial interpolation and temporal representation can affect the comparisons. However, considering the typical sea ice motion (Drucker et al., 2011) in the Weddell Sea, monthly average ULS SIT could be referred to as a spatial average value, representing 100 km around the fixed ULS positions. With the sea ice motion data from NSIDC introduced in Sect. 2.4, the 30-day origins of the sea ice passing the three ULS sites from July 2 to July 31, 2011 is shown in Fig. S1 and it is spatially representative.

3.2 Inter-comparisons between Envisat and ICESat

We first conduct an overall comparison between Envisat and ICESat effective SIT for each ICESat operating period in each season, as shown in Fig. 4–6. The effective Envisat SIT is calculated by multiplying the SIC contained in the data for each grid from OSI-SAF Global Sea Ice Concentration (OSI-409) and the OSI-SAF Global Sea Ice Concentration continuous reprocessing offline product (OSI-430) (http://osisaf.met.no). The inter-comparisons are carried out by linearly interpolating Envisat SIT onto the ICESat polar-stereographic grid with 100 km grid resolution. The results suggest that there are substantial inter-seasonal and interannual differences between the two SIT data sets.

In spring (ON), both positive and negative differences exist between Envisat and ICESat SIT (Env-ICE), shown in Fig. 4. Envisat and ICESat are both able to capture the thick ice located in the western Weddell Sea and the Bellingshausen-Amundsen Sea. Thick sea ice along the coast of the western Pacific Ocean is also detected by both sensors, but their mean SIT in 2004 are thicker than the ship-based observations (0.63 m; Worby et al., 2008a). Thin ice in the Ross Sea is not captured by Envisat (Kern et al., 2018) while the Ross Ice Shelf polynya (indicated in Fig. 2) is present in the ICESat fields. Similarly, the Ronne Ice Shelf polynya appeared only on ICESat field in 2007 but not on Envisat field. A fringe with no data along most of the East Antarctic coast is caused by ICESat data gaps, which indicates that the 100 km ICESat product fails to see the sea ice close to

the coast. This can be attributed to a different land mask used in the ICESat product and consideration of lower freeboard quality there. Table 5 provides the respective SIT and their SDs, differences, RMSDs, correlation coefficients (CCs) and the numbers of comparison pairs. In general, the difference between Envisat and ICESat spring SIT is close to zero, ranging from -0.16 m in 2006 to +0.10 m in 2007. However, these differences have to be seen in the light of the large SDs (~0.6 m) and the fact that ICESat SIT values include the snow depth. The RMSD is the smallest by 0.39 m among three seasons and CC is 0.68, with the significance larger than 95%. Note that in order to obtain the seasonal mean SIT, we compute the seasonal mean SIT only from grid cells where values are available from both data sets and available for all 3 years in autumn, at least 3 of 4 years in spring and at least 3 of 5 years in summer. The numbers of grid cells used in the calculation are listed in the last column in Table. 5.

At the end of summer melt (FM), the ice coverage is limited to the western Weddell Sea, Bellingshausen-Amundsen Sea along the coast and southern Ross Sea (Fig. 5). In the western Weddell Sea, Envisat shows that thick ice still exists and remains at least 3 m, while ICESat shows thinner ice. As for the Ross Ice Shelf polynya, ICESat displays thin ice lower than 1 m in 2004, 2007 and 2008, while Envisat detects sea ice of up to 1.5 m, much larger than expected seasonal ice thickness. According to Table 5, the numbers of comparison pairs are small. Generally, Envisat SIT exceeds ICESat SIT by 0.52 m in summer, with the largest RMSD by 0.68 m and the smallest correlation values by 0.40 among the three seasons. Considering the ICESat SIT excluding snow depth, the real differences should be larger.

In autumn (MJ), SIT patterns of the two data sets are comparable, shown in Fig. 6. The differences between Envisat and ICESat SIT are consistently positive over all regions except some regions in the Eastern Antarctic. Compared with summer, the positive differences in the western Weddell Sea expand to positive differences over the whole Weddell Sea sector, and the differences decrease from west to east. In addition, positive differences in the Ross Ice Shelf polynya still exist, mostly due to Envisat's inability to capture the thin ice there (Comiso et al., 2011; Tian et al., 2020), which has been pointed out in Kern et al. (2018) identifying a substantial SIT difference between Envisat and CryoSat-2 in that region. According to Table 5, despite the largest mean difference (0.57 m) and large RMSD (0.47 m), the correlation in autumn is actually the highest of the three seasons investigated (0.71).

To investigate the development of two SIT data from the end of melting to end of freezing, we provide the probability distribution of the Envisat SIT and the ICESat SIT for all the valid individual comparison pairs where both Envisat and ICESat have valid SIT, shown in Fig. 7. The mean and modal SIT of both data sets are marked beside. In summer, the agreement between Envisat SIT and ICESat SIT is not good, mainly due to their different performances on thick ice in the Weddell Sea (Fig. 5). Envisat still presents a larger mean and modal thickness than ICESat in autumn. In spring, the two data sets have similar distributions, represented by similar mean and modal thicknesses. In addition, we find that ICESat mean SIT increases while Envisat mean and modal SIT decreases from autumn to spring. For Envisat SIT, the distribution indicates that more ice is in thinner categories in spring than autumn, while more ice in thicker categories is found for ICESat SIT. Therefore, we

270   further compare the mean variations of Envisat SIT, ICESat SIT, Envisat freeboard, ICESat freeboard and snow depth climatology used in Envisat retrieval from autumn (MJ) to spring (ON), shown in Fig. 8. The average fields are calculated with grid cells where both Envisat and ICESat SIT have valid values in all three years from 2004 to 2006. Figure 8 shows that Envisat SIT experiences general decreases from May/June-October/November (MJON) except Bellingshausen Sea and part of Amundsen Sea. Significantly large decreases exist in Western Weddell Sea. In contrast, ICESat SIT present large-scale

275   increases except Western Weddell Sea and Ross Sea where slight decreases exist. By comparing the SIT and freeboard changes of both products, we find that the different changes of freeboard dominantly explain the SIT differences. One thing we can give a speculation based on the analyses in autumn and the regular rule during freezing seasons is that Envisat freeboard is probably overestimated in autumn, which has been pointed out in several studies before (e.g., Willatt et al., 2010; Kwok and Kacimi, 2018; Kacimi and Kwok, 2020). Moreover, the snow depth climatology also shows a decrease in Western Weddell

280   Sea and Ross Sea (Fig. 8e), which has been reported by Kern and Ozsoy-Cicek (2016) that AMSR-E snow depth is likely to underestimate the snow depth evolution during MJON, also contribute to the Envisat SIT decrease.

Figure 9 presents scatterplots of the individual comparison pairs between Envisat SIT and ICESat SIT for each region and each season. Respective CCs and RMSDs are indicated in the panels. Due to the limited measurements in the Indian Ocean and western Pacific Ocean, we combine them into the whole Eastern Antarctic. For all five sectors, Envisat SIT tends to exceed

285   ICESat SIT on thin ice. From Fig. 9a, we can see that in the western Weddell Sea, the summer and autumn SIT clouds exceed the spring ones. This reveals that ICESat SIT are nearly constant through all three seasons in the western Weddell Sea, while Envisat SIT are noticeably larger in summer and autumn, also shown in Table 6. From FM to ON, Envisat SIT changes from 3.01 m to 3.18 m to 2.23 m, while ICESat SIT changes from 2.04 m to 2.28 m to 2.23 m. Considering the regional average differences between Envisat and ICESat SIT, the largest (0.63 m) is found in the western Weddell Sea and the smallest is in

290   the Bellingshausen-Amundsen Sea (0.09 m). Differences are small in spring for all regions except Eastern Antarctic. The largest CC is found in autumn Bellingshausen-Amundsen Sea (0.58) and the smallest is in autumn Ross Sea (0.1).

4 Potential reasons for the differences

There are two main differences between the two data sets. One is the different sensors to determine surface elevation and freeboard. Envisat is equipped with a Ku-Band radar altimeter (RA-2), whose backscatter is assumed to originate from the

295   snow/ice interface. It is known that this assumption is flawed for snow that is wet, not cold and without a homogenous stratigraphy (Willatt et al., 2010). Instead, ICESat is equipped with a laser altimeter (GLAS) whose signals are reflected from the air/snow interface. In addition, considering the Envisat large pulse-limited footprint of about 2–10 km and smaller footprint of ICESat laser beams of about 70 m, there are very likely differences in the ability to resolve leads or open water required for an adequate representation of the local sea-surface height during the freeboard retrieval, as well as in the accurate representation

300   of heterogeneous sea ice surfaces. The other difference is that they apply different retrieval algorithms to convert freeboard

into thickness. Envisat directly uses the hydrostatic equilibrium together with a snow depth climatology derived from AMSR-E and AMSR2 data, while ICESat uses the hydrostatic equilibrium accompanied with a modified snow–ice density method to reduce the influence of the often regionally biased snow depth product. The effects of these differences between both products are discussed in the following.

4.1 Differences due to sensors

It is assumed that the dominant backscatter horizon for a Ku-Band radar altimeter is the snow/ice interface for cold and dry snow (Beaven et al., 1995). However, this would not always be the case in the Southern Ocean, according to the field investigations conducted by Willatt et al. (2010). They demonstrate that the dominant scattering surface of the Ku-Band radar lies within the snowpack, usually half of the mean snow depth, when the snow cover is not cold and dry. Wet conditions can affect the dielectric properties of snow and then weaken the penetration of radar altimeter signals into the snow. Consequently, RA-2 range measurements could be biased high when the main scattering horizon is located within the snow pack, which will lead to larger sea ice freeboard and larger sea ice thickness. The salinity of the basal snow layer also contributes to this effect (Nandan et al., 2017). Such biases are also shown by Kwok and Kacimi (2018), where they find that radar freeboards from CryoSat-2 are consistently higher than those computed using Operation Ice Bridge (OIB) measurements. Other studies that utilize CryoSat-2 radar data in the southern hemisphere have thus explicitly incorporated radar backscatter from the snow layer into their freeboard retrieval method (Fons and Kurtz, 2019).

The sensitivity of Envisat SIT (I) to sea ice freeboard (F) can be calculated from Eq. (1):

$$\frac{dI}{dF} = \frac{\rho_{water}}{\rho_{water} - \rho_{ice}} \tag{5}$$

We set ρ_{water} to 1024 kg m^{-3} and use ρ_{ice} between 880 and 940 kg m^{-3} to cover all mixed types of sea ice. Figure 10a illustrates the sensitivity of the sea ice thickness changes in response to sea ice density and sea ice freeboard biases between 2 and 10 cm in steps of 2 cm. We can see that SIT changes range from 14 cm to 122 cm with different freeboard biases and density in our experiment. With the increase of freeboard biases/sea ice density, SIT changes become larger. Under larger freeboard bias conditions, SIT changes climb faster as density rises. For typical sea ice freeboard biases caused by saline snow (7 cm for the Arctic nominal adjustment for first-year ice suggested by Nandan et al. (2017, 2020)), the sea ice density variations induce the thickness changes ranging from ~0.5 m to ~0.8 m. This could potentially account for the differences between Envisat and ICESat SIT in autumn (0.57 m). Therefore, we assume that in autumn freeboard-biases-induced SIT changes happen frequently. In summer, when snow salinities are significantly lower than measurements in other seasons (mostly below 0.1‰) but the wetness is high at the snow bottom (Haas et al., 2001), the freeboard biases also matters because liquid water content affects the snow dielectric properties (Barber et al., 1995). Besides, based on previous studies (Willatt et al., 2010; Kwok and Kacimi, 2018; Kacimi and Kwok, 2020), the displacements of radar retracking points and thus the freeboard biases are significant in spring. Considering the small differences between Envisat and ICESat SIT, we suggest that underestimations of snow depth

and biases in ICESat total thickness might play an important role in spring. However, detailed sensitivity discussions are limited due to lack of seasonal and regional sea ice density and adjustments to sea ice freeboard.

In addition to the different penetration depths, the two sensors have different footprints. Envisat is a pulse-limited radar altimeter with a large footprint of 2–10 km and ICESat is a laser altimeter with a small footprint of about 70 m. This makes them sensitive to a relative selection bias, primarily on the side of the altimeters with the lower resolution in the case of surface-type mixing within the footprint, especially if the different surface types vary in their backscatter properties. Higher spatial resolution will mitigate this issue and subsequently allow a better classification of lead and sea surface height retrieval in principle. Several studies have pointed that Envisat freeboard and thickness uncertainties are elevated with respect to other sensors due to sub-footprint scale surface type mixing (Schwegmann et al., 2016; Paul et al., 2018; Tilling et al., 2019). While this is also directly applicable to radar altimeters with different footprints, the response to lead surfaces of laser (ICESat) and radar (Envisat) altimeters is not directly a function of footprint size but also of altimeter concept. Leads dominate radar backscatter even if the leads are already covered by thin sea ice for nadir and off-nadir cases and thus cause an overrepresentation of lead detections with range biases for off-nadir leads in Envisat data. Off-nadir reflections are usually detected and removed from the freeboard retrieval resulting in an underrepresentation of areas with mixed surface types in the Envisat freeboard statistics. Lead laser backscatter instead is a function of the surface albedo thus leads return lower laser backscatter power and since ICESat footprints do not overlap, the lead oversampling and necessary filtering of off-nadir reflections is not an issue for laser altimetry. For variable ice surfaces, the smaller footprint of ICESat has the capability to provide more detailed observations in areas with heterogeneous ice conditions than the pulse-limited Envisat footprint.

4.2 Differences due to snow depth

Another source of the differences is the AMSR-E snow depth. AMSR-E snow depth is retrieved from brightness temperature based on the linear relation between brightness temperatures and in-situ observations (Markus and Cavalieri, 1998; Comiso et al., 2003). According to Markus and Cavalieri (1998), their AMSR-E snow depth product is limited to the maximal retrieval value being around 50 cm because of the saturation of the signal, i.e., there is no change in the brightness temperature gradient ratio with increasing snow depth over a certain limit. Previous studies show that AMSR-E snow depth tends to considerably underestimate the actual value over deformed sea ice, which usually occurs in the Eastern Antarctic (Worby et al., 2008b; Ozsoy-Cicek et al., 2011). According to Kern and Ozsoy-Cicek (2016), AMSR-E snow depths minus the ASPeCt observations is positive for snow below 15 cm and negative for snow above 30 cm. Environmental conditions have great effects on the snow physical properties such as density, wetness and salinity, and passive microwave snow depth is sensitive to ice concentration errors, weather effects, grain size, thaw and refreezing (Markus and Cavalieri, 1998). Especially, wet snow caused by melting or flooding could lead to underestimations of snow depth while refreezing of wet snow could lead to overestimations. All of the above biases can affect the differences between Envisat and ICESat SIT.

According to Eq. (1), we can derive the sensitivity of Envisat SIT (I) to snow depth (S):

$$\frac{dI}{dS} = \frac{\rho_{snow}}{\rho_{water} - \rho_{ice}} \qquad (6)$$

365   Setting $\rho_{snow} = 300$ kg m^{-3}, and taking the same values for water and sea-ice density as in Eq. 5, we can see how SIT change in response to sea ice density and snow depth biases between 5 cm and 30 cm in steps of 5 cm, shown in Fig. 10b. Thickness changes rise as snow biases get larger and also with larger sea ice density. However, compared with Fig. 10a, SIT changes are more sensitive to freeboard biases than to snow biases. For 880 kg m^{-3} density, SIT only changes 0.1 m every 5 cm snow bias but 0.14 m every 2 cm freeboard bias. With typical snow depth biases (20 cm for the monthly mean retrieval uncertainty in

370   Kern and Ozsoy-Cicek (2016)), the thickness changes from ~0.4 m to ~0.7 m. Therefore, snow depth bias is also a critical factor contributing to the difference between Envisat and ICESat SIT. In general, passive microwave snow depth is valid over level ice. During FM, snow is deep, potentially wet and/or metamorphous on thick ice, causing substantial difficulties for radar altimeters. And for the same reasons, passive microwave snow depth is possibly underestimated on thick ice during FM but also during other seasons. These snow depths also underestimate actual snow depth over deformed ice mostly during ON in

375   Eastern Antarctic, Bellingshausen and Amundsen Seas (Kwok and Maksym, 2014; Kacimi and Kwok, 2020).

Additionally, more significant effects might come from the differences between actual snow depth from that represented by the climatology. During the Envisat SIT retrieval, the snow depth climatology is employed neglecting the inter-annual snow variability. According to Bunzel et al. (2018), the impact of using a snow depth climatology is small when the snow depth is thin. The usage of snow depth climatology allows reducing the relative uncertainties compared with using the actual snow

380   depth values. The latter ones are affected by many factors as discussed above and have large uncertainties. However, it can also have an adverse effect when being constructed from biased snow depth data, as is the case for the climatology used for the Envisat SIT data. To further quantify the differences between snow depth climatology and actual snow depth contributions, we conduct the retrieval of Envisat SIT by replacing the snow depth climatology with monthly SICCI AMSR-E snow depth provided by SICCI (Kern et al., 2015). The new Envisat SIT is converted through Eq. (1) with Envisat monthly gridded sea

385   ice freeboard data, monthly AMSR-E snow depth and the same density values mentioned above. The new Envisat SIT is compared with ICESat SIT and the changes to former Envisat-ICESat differences are shown in Table. S1. This result reveals that the impacts of snow depth climatology are larger in the Amundsen-Bellingshausen Sea and the Western Weddell Sea compared to other sectors. Among the three seasons, the changes are larger in summer, partly accounting for the differences between Envisat and ICESat SIT.

390   Moreover, the distance between sea ice surface elevations and the sea surface height is computed with vacuum light speed, which is defined as radar freeboard (RFB). A geometric correction used to correct the slower wave propagation speed in the snow layer is applied to convert the radar freeboard into the sea ice freeboard (FB):

$$FB = RFB + 0.22 \times SD \tag{7}$$

But the delay correction is based on a conventional assumption that has been assessed by Mallett et al. (2019), which pointed out that it introduced systematic underestimation of up to 15 cm into SIT estimates. While this systematic bias is small compared to other sources, uncertainties of snow depths and incomplete radar wave penetration would cause larger biases in this way.

4.3 Differences due to ICESat biases

The modified density method used by Kern et al. (2016) does not consider the small-scale or regional variability of the snow depth. Instead, only a seasonal constant density derived from the ASPeCt observations is given. Therefore, the largest uncertainty of ICESat comes from the potential underestimations of the ship-based sea ice thickness and snow depth observations for the computation of the bulk density of the ice-snow column (Kern et al., 2016). This bias has been modified in Li et al. (2018), who derived first guess values of snow depth and sea ice thickness directly from ICESat data with empirical approaches, instead of the observation climatology used by Kern et al. (2016). Besides, this method is actually providing the total (sea ice plus snow depth) thickness. Taking this into account, the actual ICESat SIT shown in this paper would possibly even be a bit smaller. To examine this issue, we subtract the snow depth climatology (used in Envisat retrieval) from the ICESat data and compare them with Envisat thickness. The changes to the former differences are shown in Table. S2, which is also a representation of the snow depth climatology itself. Larger variations exist in the Western Weddell Sea, especially in summer and autumn. The general variations are smaller than 0.5 m, yet leading to larger positive differences between Envisat and ICESat SIT. More realistic SIT data are derived in Xu et al. (2021) by subtracting the snow depth. However, we do not aim to choose the best ICESat SIT product with the most real SIT, but investigate the causes of the differences between Envisat and ICESat SIT, and how different sensors and retrieval methods are represented in the SIT fields.

Apart from the uncertainties from ICESat retrieval method mentioned above, Kern et al. (2016) also discussed the potential biases due to total freeboard and sea ice density. In comparison with the freeboard from Kurtz and Markus (2012), modal and mean total freeboard values of this product are slightly higher, which might be a potential source of SIT positive biases. The total freeboard retrieved from ICESat has an uncertainty of up to 0.1 m, mainly due to the choice of percentage of observations used as sea surface height tie points (Kern and Spreen, 2015). Meanwhile, a smaller sea ice density will lead to smaller modified ice-snow density and SIT according to Eq. (2) and Eq. (3). We analyse the sensitivity of ICESat SIT to sea ice density and find an increase of ~0.2–0.4 m SIT when sea ice density rises from 880 to 940 kg m^{-3} under seasonal R values and total freeboard.

5 Summary

In this study, we compare SIT estimates of the sea-ice thickness obtained from satellite altimeter observations by Envisat RA-2 (radar) and ICESat GLAS (laser) in the Southern Ocean. Envisat and ICESat SIT are compared with ULS SIT in the Weddell

Sea, with the MDs (SDs) of 1.29 (0.65) m for Envisat-ULS while 1.11 (0.81) m for ICESat-ULS, respectively. Then a systematic comparison between the two data sets is carried out for three seasons except winter, based on the ICESat operating

425 periods. According to the results, the differences between Envisat and ICESat SIT vary in each season, year and region. More specifically, the smallest monthly average difference (SD in brackets) for Envisat SIT minus ICESat SIT exists in spring of 0.00 m (0.39 m), while larger differences (SD) exist in summer and autumn by 0.52 m (0.68 m) and 0.57 m (0.45 m), respectively. In spring, ICESat SIT fields reveal the Ross Ice Shelf polynya, while it is not present in the Envisat data. In summer, Envisat shows that thick ice still exists in the western Weddell Sea and remains at least 3 m thick every year, while

430 ICESat shows thinner ice. Compared to summer, the positive differences in the western Weddell Sea expand to the whole Weddell Sea sector and slightly decrease from west to east in autumn. From the probability distribution, it is noted that Envisat and ICESat have different SIT variations from autumn to spring, i.e., ICESat SIT increases while Envisat SIT does not, but share similar SIT growth from summer to autumn. Compared to the average changes of Envisat freeboard, ICESat freeboard and snow depth climatology used in Envisat retrieval during MJON calculated from 2004, 2005 and 2006, we assume the main

435 reason of the Envisat SIT decrease is the overestimation of Envisat freeboard in autumn and the underestimation of snow depth evolution during MJON. With respect to different sectors, the regional MDs (SDs) are 0.63 m (0.91 m) in the Western Weddell Sea, 0.34 m (0.58 m) in the Eastern Weddell Sea, 0.31 m (0.57 m) in the Ross Sea, -0.12 m (0.69 m) in the Eastern Antarctic, and 0.09 m (0.71 m) in the Bellingshausen-Amundsen Sea. Through the sensitivity experiments, we find that Envisat SIT changes are more sensitive to sea ice freeboard biases than to snow depth biases. Besides, with the increase of sea ice density,

440 the SIT changes become larger. Usage of snow depth climatology has moderate impacts on SIT estimates in summer Amundsen-Bellingshausen Sea and Western Weddell Sea. Moreover, ICESat SIT can have an increase of ~0.2–0.4 m when sea ice density rises from 880 to 940 kg m^{-3} under seasonal R values and total freeboard.

While we choose one of the ICESat SIT products to conduct the comparison, there are many other ICESat SIT products using different retrieval algorithms available, e.g., the SICCI product discriminating between positive and negative sea ice freeboard

445 (Kern et al., 2016), or the one assuming zero sea ice freeboard in freeboard-to-thickness conversion (Kurtz and Markus, 2012). These different products provide a range of values within which ICESat SIT may be located, thus the differences between Envisat and ICESat SIT in this study are just one of the possible outcomes.

Through the study, we acknowledge that there are differences between Envisat and ICESat sea ice thickness, which potentially result from the biases of both data sets. There is still more work to be done in the future to make better use of remote-sensed

450 SIT data, such as assimilating the Antarctic sea ice thickness observations and analyzing the sea ice volume variations.

Data availability. Envisat sea ice thickness data are available at https://dx.doi.org/10.5285/b1f1ac03077b4aa784c5a413a2210bf5 (Hendricks et al., 2018b). ICESat-1 sea ice thickness data are available at http://icdc.cen.uni-hamburg.de/1/projekte/esa-cci-sea-ice-ecv0/esa-cci-data-access-form-antarctic-sea-ice-

thickness.html (Kern et al., 2016). The Weddell Sea upward looking sonar data are available
at http://doi.pangaea.de/10.1594/PANGAEA.785565 (Behrendt et al., 2013a; Behrendt et al., 2013b). NSIDC sea ice motion
data are accessible at https://nsidc.org/data/nsidc-0116 (Tschudi et al., 2019). AMSR-E snow depth data are accessible at
https://www.cen.uni-hamburg.de/icdc (Markus and Cavalieri, 1998).

Author contributions. QS developed the concept of the paper. JW analyzed the data and wrote the manuscript. CM, RR, QS, BH, SH, RW and QY assisted during the writing process.

Acknowledgments. This study is supported by the National Natural Science Foundation of China (No. 41941009, 41922044), the Guangdong Basic and Applied Basic Research Foundation (No. 2020B1515020025), and the fundamental research funds for the Norges Forskningsråd. (No. 328886). The authors would like to thank Alfred Wegener Institute Helmholtz Centre for Polar and Marine Research for providing the Weddell Sea upward looking sonar data, the Integrated Climate Data Center at the University of Hamburg for providing the ICESat-1 sea ice thickness data.

References

Barber, D. G., Reddan, S. P., and LeDrew, E. F.: Statistical characterization of the geophysical and electrical properties of snow on Landfast first-year sea ice, J. Geophys. Res., 100 (C2), 2673– 2686, https://doi.org/10.1029/94JC02200, 1995.

Beaven, S. G., Lockhart, G. L., Gogineni, S. P., Hossetnmostafa, A. R., Jezek, K., Gow, A. J., Perovich, D. K., Fung, A. K., and Tjuatja, S.: Laboratory measurements of radar backscatter from bare and snow-covered saline ice sheets, Int. J. Remote Sens., 16, 851–876, https://doi.org/10.1080/01431169508954448, 1995.

Behrendt, A.: The Sea Ice Thickness in the Atlantic Sector of the Southern Ocean, Ph.D. thesis, University of Bremen, Germany, 239 pp., 2013.

Behrendt, A., Dierking, W., Fahrbach, E., and Witte, H.: Sea ice draft measured by upward looking sonars in the Weddell Sea (Antarctica), PANGAEA, https://doi.org/10.5194/PANGAEA.785565, 2013a.

Behrendt, A., Dierking, W., Fahrbach, E., and Witte, H.: Sea ice draft in the Weddell Sea, measured by upward looking sonars, Earth Syst. Sci. Data, 5, 209–226, https://doi.org/10.5194/essd-5-209-2013, 2013b.

Belter, H. J., Krumpen, T., Hendricks, S., Hoelemann, J., Janout, M. A., Ricker, R., and Haas, C.: Satellite-based sea ice thickness changes in the Laptev Sea from 2002 to 2017: comparison to mooring observations, The Cryosphere, 14, 2189–2203,

480   https://doi.org/10.5194/tc-14-2189-2020, 2020.

Bunzel, F., Notz, D., and Pedersen, L. T.: Retrievals of Arctic Sea-Ice Volume and Its Trend Significantly Affected by Interannual Snow Variability, Geophys. Res. Lett., 45(21), 11,751-11,759. https://doi.org/10.1029/2018GL078867, 2018.

Cavalieri, D. J., Markus T., and Comiso J. C.: AMSR-E/Aqua Daily L3 12.5 km Brightness Temperature, Sea Ice Concentration, & Snow Depth Polar Grids, Version 3, Boulder, Colorado USA. NASA National Snow and Ice Data Center

485   Distributed Active Archive Center. http://dx.doi.org/10.5067/AMSR-E/AE_SI12.003, 2014.

Comiso, J. C., Cavalieri, D. J., and Markus, T.: Sea ice concentration, ice temperature, and snow depth using AMSR-E data, IEEE Trans. Geosci. Remote Sens., 41, 243–252, https://doi.org/10.1109/TGRS.2002.808317, 2003.

Comiso, J. C., Kwok, R., Martin, S., and Gordon, A. L.: Variability and trends in sea ice extent and ice production in the Ross Sea, J. Geophys. Res., 116, C04021, https://doi.org/10.1029/2010JC006391, 2011.

490   Comiso, J. C., Gersten, R. A., Stock, L. V., Turner, J., Perez, G. J., and Cho, K.: Positive Trend in the Antarctic Sea Ice Cover and Associated Changes in Surface Temperature, J. Climate, 30, 2251–2267, https://doi.org/10.1175/JCLI-D-16-0408.1, 2017.

Connor, L. N., Laxon, S. W., Ridout, A. L., Krabill, W. B., and McAdoo, D. C.: Comparison of Envisat radar and airborne laser altimeter measurements over Arctic sea ice, Remote Sens. Environ., 113, 563–570, https://doi.org/10.1016/j.rse.2008.10.015, 2009.

495   Copernicus Climate Change Service (C3S) (2017): ERA5: Fifth generation of ECMWF atmospheric reanalyses of the global climate. Copernicus Climate Change Service Climate Data Store (CDS), date of access. https://cds.climate.copernicus.eu/cdsapp#!/home

Drucker, R., Martin, S., and Kwok, R.: Sea ice production and export from coastal polynyas in the Weddell and Ross Seas, Geophys. Res. Lett., 38, L17502, https://doi.org/10.1029/2011GL048668, 2011.

500   El Naggar, S. E. D., Dieckmann, G., Haas, C., Schröder, M., and Spindler, M.: The Expeditions ANTARKTIS-XXII/1 and XII/2 of the Research Vessel" Polarstern" in 2004/2005, Reports on Polar and Marine Research, 551, 268 pp., 2007.Fons, S. W. and Kurtz, N. T.: Retrieval of snow freeboard of Antarctic sea ice using waveform fitting of CryoSat-2 returns, The Cryosphere, 13, 861–878, https://doi.org/10.5194/tc-13-861-2019, 2019.

Giles, K. A., Laxon, S. W., and Worby, A. P.: Antarctic sea ice elevation from satellite radar altimetry, Geophys. Res. Lett., 35, https://doi.org/10.1029/2007GL031572, 2008.

Goosse, H. and Zunz, V.: Decadal trends in the Antarctic sea ice extent ultimately controlled by ice–ocean feedback, The Cryosphere, 8, 453–470, https://doi.org/10.5194/tc-8-453-2014, 2014.

Lebedev, V. V.: The dependence between growth of ice in Arctic rivers and seas and negative air temperature (in Russian). Probl. Arkt. 5-6, 9-25, 1938.

Haas, C., Thomas, D., and Bareiss, J.: Surface properties and processes of perennial Antarctic sea ice in summer, Journal of Glaciology, 47(159), 613-625, https://doi.org/10.3189/172756501781831864, 2001.

Harms, S., Fahrbach, E., and Strass, V. H.: Sea ice transports in the Weddell Sea, J. Geophys. Res., 106, 9057–9073, https://doi.org/10.1029/1999JC000027, 2001.

Hendricks, S., Paul, S., Rinne, E.: ESA Sea Ice Climate Change Initiative (Sea_Ice_cci): Southern hemisphere sea ice thickness from the CryoSat-2 satellite on a monthly grid (L3C) v2.0, Centre for Environmental Data Analysis, https://dx.doi.org/10.5285/48fc3d1e8ada405c8486ada522dae9e8, 2018a.

Hendricks, S., Paul, S., Rinne, E.: ESA Sea Ice Climate Change Initiative (Sea_Ice_cci): Southern hemisphere sea ice thickness from the Envisat satellite on a monthly grid (L3C) v2.0, Centre for Environmental Data Analysis, https://dx.doi.org/10.5285/b1f1ac03077b4aa784c5a413a2210bf5, 2018b.

Hendricks, S., Stenseng, L., Helm, V., and Haas, C.: Effects of surface roughness on sea ice freeboard retrieval with an Airborne Ku-Band SAR radar altimeter, 2010 IEEE International Geoscience and Remote Sensing Symposium, Honolulu, HI, USA, 25–30 July 2010, 3126–3129, 2010.

Kacimi, S. and Kwok, R.: The Antarctic sea ice cover from ICESat-2 and CryoSat-2: freeboard, snow depth, and ice thickness, The Cryosphere, 14, 4453–4474, https://doi.org/10.5194/tc-14-4453-2020, 2020.

Kaleschke, L., Lüpkes, C., Vihma, T., Haarpaintner, J., Bochert, A., Hartmann, J., and Heygster, G.: SSM/I sea ice remote sensing for meoscale ocean-atmosphere interaction analysis., Canad. J. Rem. Sens., 27, 526-537, https://doi.org/10.1080/07038992.2001.10854892, 2001.

Kern, S., and Ozsoy-Cicek, B.: Satellite Remote Sensing of Snow Depth on Antarctic Sea Ice: An Inter-Comparison of Two Empirical Approaches. Remote Sens., 8, 450, https://doi.org/10.3390/rs8060450, 2016.

530 Kern, S., and Spreen, G.: Uncertainties in Antarctic sea-ice thickness retrieval from ICESat, Ann. Glaciol., 56, 107–119, https://doi.org/10.3189/2015AoG69A736, 2015.

Kern, S., Frost, T., and Heygster, G.: D1.3 Product User Guide (PUG) for Antarctic AMSR-E snow depth product SD v1.1, available at : https://icdc.cen.uni-hamburg.de/fileadmin/user_upload/ESA_Sea-Ice-ECV/SICCI_ANT_SIT_Option_PUG_D1.3_Issue_2.1_final.pdf, 2015.

535 Kern, S., Ozsoy-Çiçek, B., and Worby, A. P.: Antarctic sea-ice thickness retrieval from ICESat: Inter-comparison of different approaches, Remote Sens., 8, 538, https://doi.org/10.3390/rs8070538, 2016.

Kern, S., Khvorostovsky K., and Skourup, H.: D4.1 Product Validation & Intercomparison Report (PVIR-SIT), available at: http://icdc.cen.uni-hamburg.de/fileadmin/user_upload/ESA_Sea-Ice-ECV_Phase2/SICCI_P2_PVIR-SIT_D4.1_Issue_1.1.pdf, 2018.

540 Koenig, L., Martin, S., Studinger, M., and Sonntag, J.: Polar Airborne Observations Fill Gap in Satellite Data, Eos Trans. Amer. Geophys. Union, 91, 333–334, https://doi.org/10.1029/2010EO380002, 2010.

Kurtz, N. T., and Markus, T.: Satellite observations of Antarctic sea ice thickness and volume, J. Geophys. Res., 117, https://doi.org/10.1029/2012JC008141, 2012.

Kwok, R. and Kacimi, S.: Three years of sea ice freeboard, snow depth, and ice thickness of the Weddell Sea from Operation
545 IceBridge and CryoSat-2, The Cryosphere, 12, 2789–2801, https://doi.org/10.5194/tc-12-2789-2018, 2018.

Kwok, R., and Maksym, T.: Snow depth of the Weddell and Bellingshausen sea ice covers from IceBridge surveys in 2010 and 2011: An examination, J. Geophys. Res., 119, 4141-4167, https://doi.org/10.1002/2014JC009943, 2014.

Kwok, R., Zwally, H. J., and Yi, D.: ICESat observations of Arctic sea ice: A first look, Geophys. Res. Lett., 31, L16401, https://doi.org/10.1029/2004GL020309, 2004.

550 Kwok, R., G. F. Cunningham, T. Markus, D. Hancock, J. Morison, S. Palm, et al.: ATLAS/ICESat-2 L3A Sea Ice Height, Version 1. Boulder, Colorado USA. NSIDC: National Snow and Ice Data Center. https://doi.org/10.5067/ATLAS/ATL07.001, 2019.

Landy, J. C., Petty, A. A., Tsamados, M., and Stroeve, J. C.: Sea Ice Roughness Overlooked as a Key Source of Uncertainty in CryoSat-2 Ice Freeboard Retrievals, J. Geophys. Res., 125, e2019JC015820, https://doi.org/10.1029/2019JC015820, 2020.

Laxon, S., Peacock, N., and Smith, D.: High interannual variability of sea ice thickness in the Arctic region, Nature, 425, 947-950, https://doi.org/10.1038/nature02050, 2003.

Lemke, P.: The expedition of the research vessel" Polarstern" to the Antarctic in 2006 (ANT-XXIII/7), Reports on Polar and Marine Research, 586, 147 pp., 2009.

Lemke, P.: The Expedition of the Research Vessel Polarstern to the Antarctic in 2013 (ANT-XXIX/6), Reports on Polar and Marine Research, 679, 1-154, https://doi.org/10.2312/BzPM_0679_2014

Li, H., Xie, H., Kern, S., Wan, W., Ozsoy, B., Ackley, S., and Hong, Y.: Spatio-temporal variability of Antarctic sea-ice thickness and volume obtained from ICESat data using an innovative algorithm, Remote Sens. Environ., 219, 44-61, https://doi.org/https://doi.org/10.1016/j.rse.2018.09.031, 2018.

Maksym, T.: Arctic and Antarctic Sea Ice Change: Contrasts, Commonalities, and Causes, Annu. Rev. Mar. Sci., 11, 187–213, https://doi.org/10.1146/annurev-marine-010816-060610, 2019.

Mallett, R. D. C., Lawrence, I. R., Stroeve, J. C., Landy, J. C., and Tsamados, M.: Brief communication: Conventional assumptions involving the speed of radar waves in snow introduce systematic underestimates to sea ice thickness and seasonal growth rate estimates, The Cryosphere, 14, 251–260, https://doi.org/10.5194/tc-14-251-2020, 2020.

Markus, T., and Cavalieri, D. J.: Snow Depth Distribution Over Sea Ice in the Southern Ocean from Satellite Passive Microwave Data, in Antarctic Sea Ice: Physical Processes, Interactions and Variability, edited by: M. O. Jeffries, AGU, Washington, D. C., 19–39, https://doi.org/doi:10.1029/AR074p0019, 1998.

Markus, T., Massom, R., Worby, A., Lytle, V., Kurtz, N., and Maksym, T.: Freeboard, snow depth and sea-ice roughness in East Antarctica from in situ and multiple satellite data, Ann. Glaciol., 52, 242–248, https://doi.org/10.3189/172756411795931570, 2011.

Massom, R. A., Eicken, H., Haas, C., Jeffries, M. O., Drinkwater, M. R., Sturm, M., Worby, A. P., Wu, X. R., Lytle, V. I., Ushio, S., Morris, K., Reid, P. A., Warren, S. G., and Allison, I.: Snow on Antarctic Sea ice, Rev. Geophys., 39, 413–445, 2001.

Massom, R. A., Scambos, T. A., Bennetts, L. G., Reid, P., Squire, V. A., and Stammerjohn, S. E.: Antarctic ice shelf disintegration triggered by sea ice loss and ocean swell, Nature, 558, 383–389, https://doi.org/10.1038/s41586-018-0212-1, 2018.

Massonnet, F., Mathiot, P., Fichefet, T., Goosse, H., König Beatty, C., Vancoppenolle, M., and Lavergne, T.: A model reconstruction of the Antarctic sea ice thickness and volume changes over 1980–2008 using data assimilation, Ocean Model., 64, 67-75, https://doi.org/https://doi.org/10.1016/j.ocemod.2013.01.003, 2013.

585 McLaren, A. J., Banks, H. T., Durman, C. F., Gregory, J. M., Johns, T. C., Keen, A. B., Ridley, J. K., Roberts, M. J., Lipscomb, W. H., Connolley, W. M., and Laxon, S. W.: Evaluation of the sea ice simulation in a new coupled atmosphere-ocean climate model (HadGEM1), J. Geophys. Res., 111, https://doi.org/10.1029/2005JC003033, 2006.

Meiners, K. M., Vancoppenolle, M., Thanassekos, S., Dieckmann, G. S., Thomas, D. N., Tison, J. L., Arrigo, K. R., Garrison, D. L., McMinn, A., Lannuzel, D., van der Merwe, P., Swadling, K. M., Smith Jr, W. O., Melnikov, I., and Raymond, B.: Chlorophyll a in Antarctic sea ice from historical ice core data, Geophys. Res. Lett., 39, 590 https://doi.org/10.1029/2012GL053478, 2012.

Nandan, V., Geldsetzer, T., Yackel, J., Mahmud, M., Scharien, R., Howell, S., King, J., Ricker, R., and Else, B.: Effect of Snow Salinity on CryoSat-2 Arctic First-Year Sea Ice Freeboard Measurements, Geophys. Res. Lett., 44, 10,419-10,426, https://doi.org/10.1002/2017GL074506, 2017.

Nandan, V., Scharien, R. K., Geldsetzer, T., Kwok, R., Yackel, J. J., Mahmud, M. S., Rosel, A., Tonboe, R., Granskog, M., 595 Willatt, R., Stroeve, J., Nomura, D., and Frey, M.: Snow Property Controls on Modeled Ku-Band Altimeter Estimates of FirstYear Sea Ice Thickness: Case Studies from the Canadian and Norwegian Arctic, IEEE J. Sel. Top. Appl., 13, 1082–1096, https://doi.org/10.1109/jstars.2020.2966432, 2020.

Nihashi, S., and Ohshima, K. I.: Circumpolar Mapping of Antarctic Coastal Polynyas and Landfast Sea Ice: Relationship and Variability, J. Climate, 28, 3650–3670, https://doi.org/10.1175/JCLI-D-14-00369.1, 2015.

600 Ozsoy-Cicek, B., Kern, S., Ackley, S. F., Xie, H., and Tekeli, A. E.: Intercomparisons of Antarctic sea ice types from visual ship, RADARSAT-1 SAR, Envisat ASAR, QuikSCAT, and AMSR-E satellite observations in the Bellingshausen Sea, Deep-Sea Res. II, 58, 1092–1111, https://doi.org/https://doi.org/10.1016/j.dsr2.2010.10.031, 2011.

Parkinson, C. L., and Cavalieri, D. J.: Antarctic sea ice variability and trends, 1979–2010, The Cryosphere, 6, 871–880, https://doi.org/10.5194/tc-6-871-2012, 2012.

605 Parkinson, C. L., and DiGirolamo, N. E.: Sea ice extents continue to set new records: Arctic, Antarctic, and global results, Remote Sensing of Environment, 267, 112753, https://doi.org/10.1016/j.rse.2021.112753, 2021.

Paul, S., Hendricks, S., and Rinne, E.: Sea Ice Thickness Algorithm Theoretical Basis Document (ATBD), v1.0, ESA Climate Change Initiative on Sea Ice (SICCI), https://icdc.cen.uni-hamburg.de/fileadmin/user_upload/ESA_Sea-Ice-ECV_Phase2/SICCI_P2_ATBD_D2.1__SIT__Issue_1.0.pdf, 2017.

610 Paul, S., Hendricks, S., Ricker, R., Kern, S., and Rinne, E.: Empirical parametrization of Envisat freeboard retrieval of Arctic and Antarctic sea ice based on CryoSat-2: progress in the ESA Climate Change Initiative, The Cryosphere, 12, 2437–2460, https://doi.org/10.5194/tc-12-2437-2018, 2018.

Peacock, N. R. and Laxon, S. W.: Sea surface height determination in the Arctic Ocean from ERS altimetry, J. Geophys. Res., 109, C07001, https://doi.org/10.1029/2001JC001026, 2004.

615 Ricker, R., Hendricks, S., Helm, V., Skourup, H., and Davidson, M.: Sensitivity of CryoSat-2 Arctic sea-ice freeboard and thickness on radar-waveform interpretation, The Cryosphere, 8, 1607–1622, https://doi.org/10.5194/tc-8-1607-2014, 2014.

Schwegmann, S., Rinne, E., Ricker, R., Hendricks, S., and Helm, V.: About the consistency between Envisat and CryoSat-2 radar freeboard retrieval over Antarctic sea ice, The Cryosphere, 10, 1415–1425, https://doi.org/10.5194/tc-10-1415-2016, 2016.

620 Tian, L., Xie, H., Ackley, S., Tang, J., Mestas-Nuñez, A., and Wang, X.: Sea-ice freeboard and thickness in the Ross Sea from airborne (IceBridge 2013) and satellite (ICESat 2003–2008) observations, Ann. Glaciol., 61(82), 24-39, https://doi.org/10.1017/aog.2019.49, 2020.

Tilling, R., Ridout, A., and Shepherd, A.: Assessing the Impact of Lead and Floe Sampling on Arctic Sea Ice Thickness Estimates from Envisat and CryoSat-2, J. Geophys. Res., 124, 7473–7485, https://doi.org/10.1029/2019JC015232, 2019.

625 Tschudi, M., Meier W. N., Stewart J. S., Fowler C., and Maslanik J.: Polar Pathfinder Daily 25 km EASE-Grid Sea Ice Motion Vectors, Version 4. Boulder, Colorado USA. NASA National Snow and Ice Data Center Distributed Active Archive Center. https://doi.org/10.5067/INAWUWO7QH7B, 2019.

Turner, J., and Comiso, J.: Solve Antarctica's sea-ice puzzle, Nature, 547, 275–277, https://doi.org/10.1038/547275a, 2017.

Wang, X., Jiang, W., Xie, H., Ackley, S., and Li, H.: Decadal variations of sea ice thickness in the Amundsen-630 Bellingshausen and Weddell seas retrieved from ICESat and IceBridge laser altimetry, 2003–2017. J. Geophys. Res., 125, e2020JC016077, https://doi.org/10.1029/2020JC016077, 2020.

Willatt, R. C., Giles, K. A., Laxon, S. W., Stone-Drake, L., and Worby, A. P.: Field Investigations of Ku-Band Radar Penetration into Snow Cover on Antarctic Sea Ice, IEEE Trans. Geosci. Remote Sens., 48, 365–372, https://doi.org/10.1109/TGRS.2009.2028237, 2010.

635   Williams, G., Maksym, T., Wilkinson, J., Kunz, C., Murphy, C., Kimball, P., and Singh, H.: Thick and deformed Antarctic sea ice mapped with autonomous underwater vehicles, Nature Geosci., 8, 61–67, https://doi.org/10.1038/ngeo2299, 2015.

Worby, A. P., Geiger, C. A., Paget, M. J., Van Woert, M. L., Ackley, S. F., and DeLiberty, T. L.: Thickness distribution of Antarctic sea ice, J. Geophys. Res., 113, https://doi.org/10.1029/2007JC004254, 2008a.

Worby, A. P., Markus, T., Steer, A. D., Lytle, V. I., and Massom, R. A.: Evaluation of AMSR-E snow depth product over East
640   Antarctic sea ice using in situ measurements and aerial photography, J. Geophys. Res., 113, https://doi.org/10.1029/2007JC004181, 2008b.

Xie, H., Tekeli, A. E., Ackley, S. F., Yi, D., and Zwally, H. J.: Sea ice thickness estimations from ICESat Altimetry over the Bellingshausen and Amundsen Seas, 2003–2009, J. Geophys. Res., 118, 2438–2453, https://doi.org/10.1002/jgrc.20179, 2013.

Yi, D., Zwally, H. J., and Robbins, J. W.: ICESat observations of seasonal and interannual variations of sea-ice freeboard and
645   estimated thickness in the Weddell Sea, Antarctica (2003–2009), Ann. Glaciol., 52, 43–51, https://doi.org/10.3189/172756411795931480, 2011.

Zelli, C., and Aerospazio, A.: ENVISAT RA-2 advanced radar altimeter: Instrument design and pre-launch performance assessment review, Acta Astronaut., 44, 323–333, https://doi.org/https://doi.org/10.1016/S0094-5765(99)00063-6, 1999.

Zhang, J.: Increasing Antarctic Sea Ice under Warming Atmospheric and Oceanic Conditions, J. Climate, 20, 2515–2529,
650   https://doi.org/10.1175/JCLI4136.1, 2007.
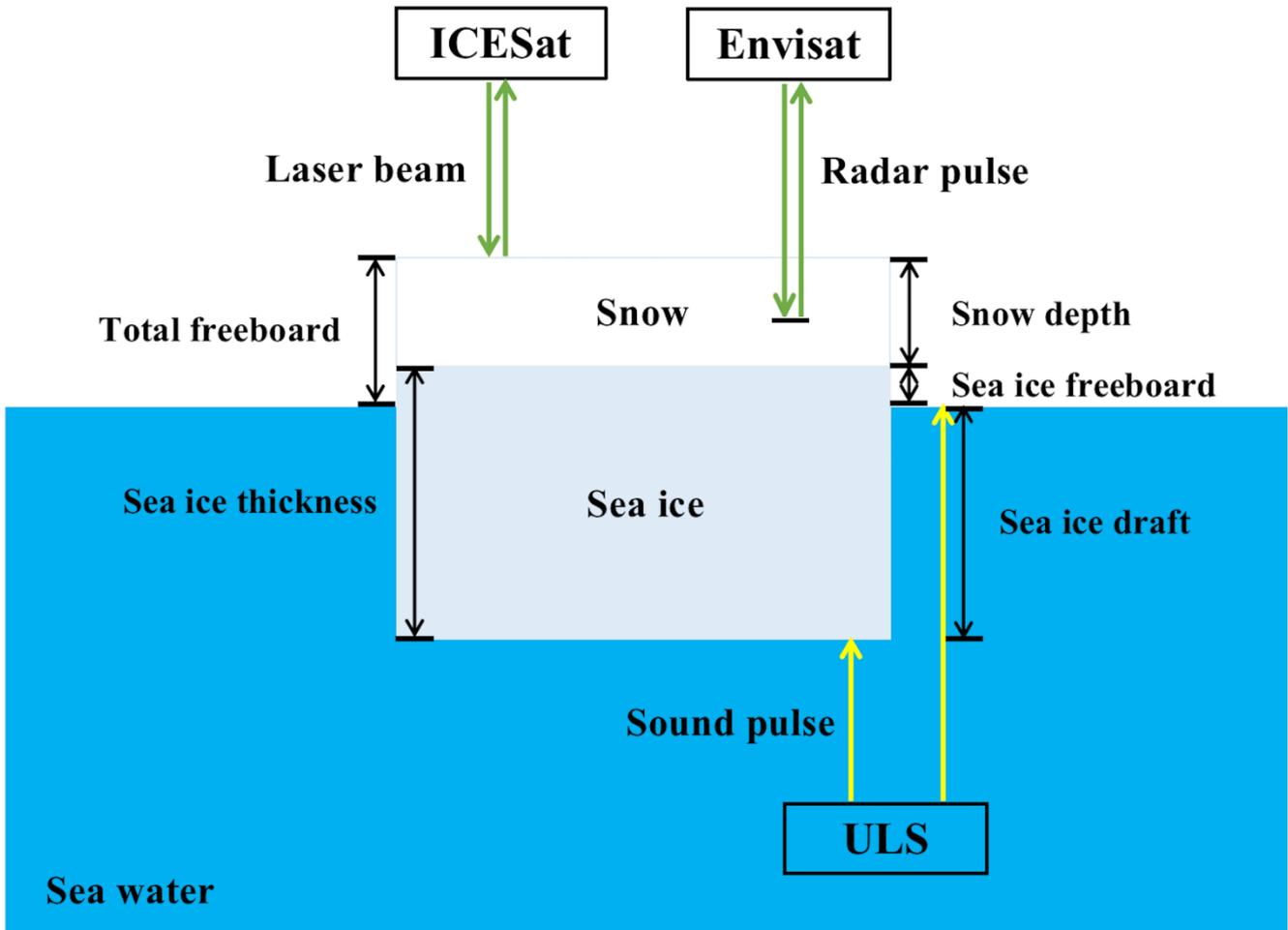
Figure 1: An illustration of measuring freeboard using ICESat and Envisat, and the ULS measurement principle. Noted that radar altimeter on Envisat usually penetrates to somewhere between the air/snow and snow/ice interfaces (Willatt et al., 2010).
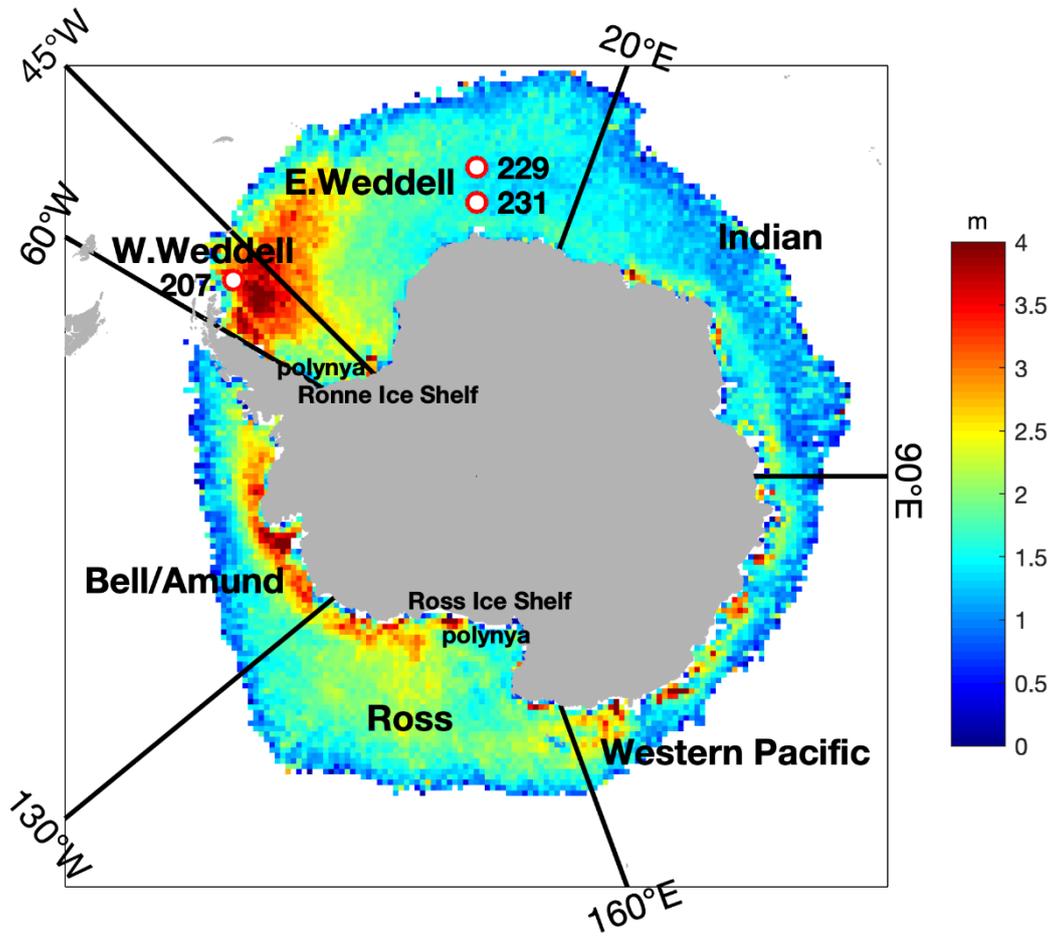
Figure 2: Map of the different sectors referred to in the study. The background is the average of the September sea ice thickness from Envisat during 2003-2011 with 50 km grid size. Each sector and the two ice shelf polynyas are indicated in the figure. The circles and the corresponding numbers refer to the sites of the ULS. The white grid cells stand for area with sea ice concentration less than 70% or missing data.
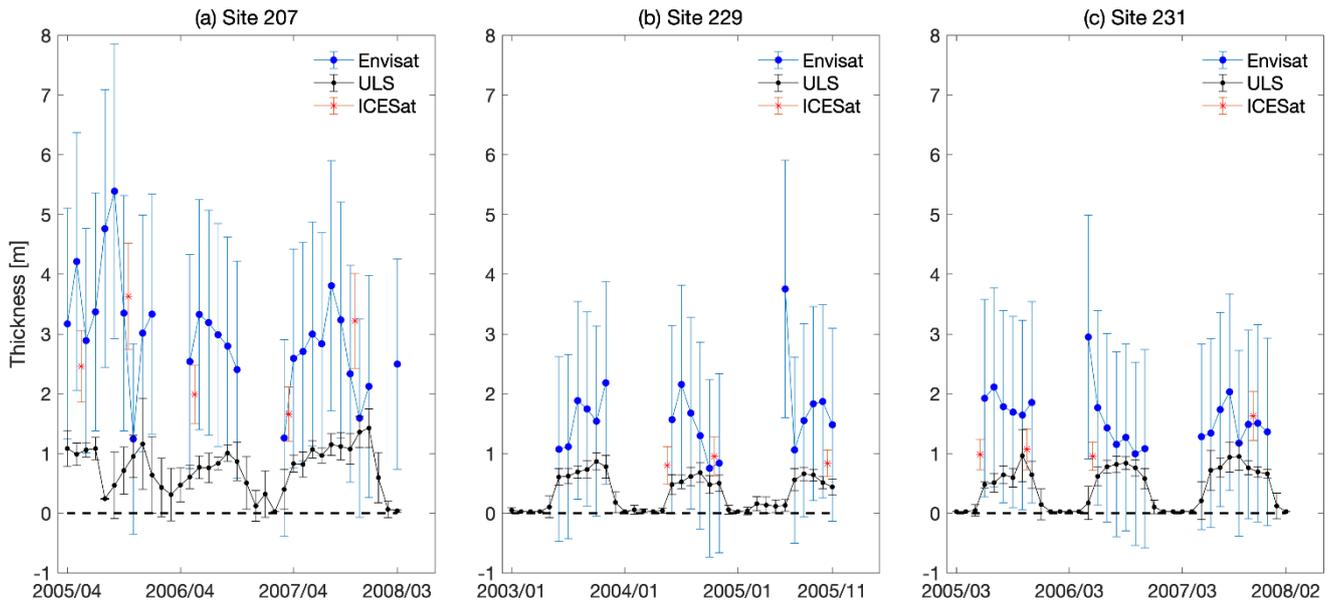
Figure 3: Time series of sea ice thickness and their uncertainties for the Weddell Sea ULS data, Envisat and ICESat. The numbers on the top represent the location of each site for the comparisons. The site locations can be searched in Fig. 2. ICESat SIT values are placed between the two months that each period covers.
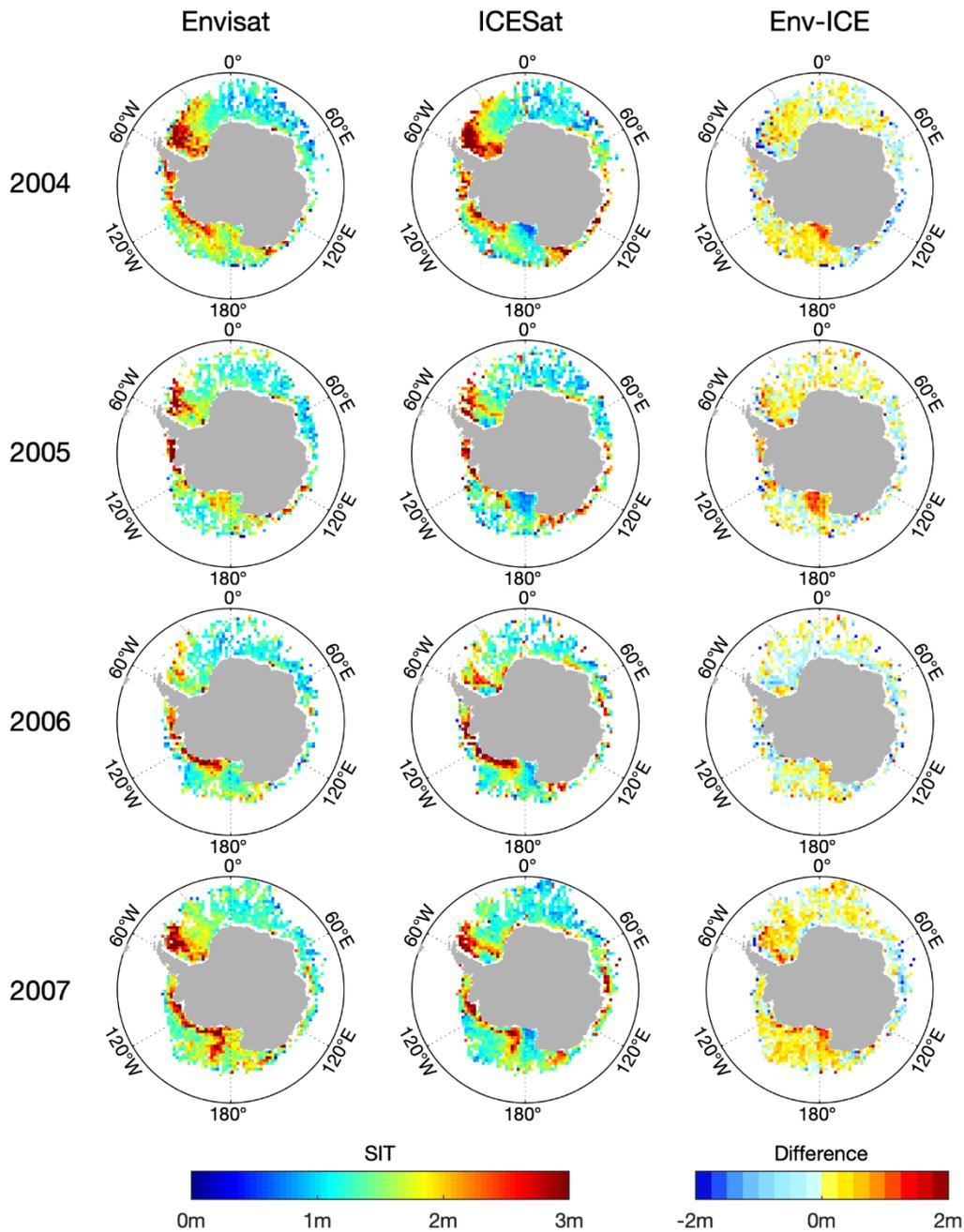
Figure 4: Comparisons of Envisat versus ICESat sea ice thickness for each ICESat operating period in spring (October & November). The first and second columns show the sea ice thickness distribution of Envisat and ICESat respectively, and the last column shows the difference field (Envisat minus ICESat) of sea ice thickness. Each row represents a year from 2004 to 2007. The maps are all interpolated onto the polar-stereographic grid of the ICESat product and only show grid cells where both data have valid SIT. The white cells denote sea ice concentration less than threshold or missing data.
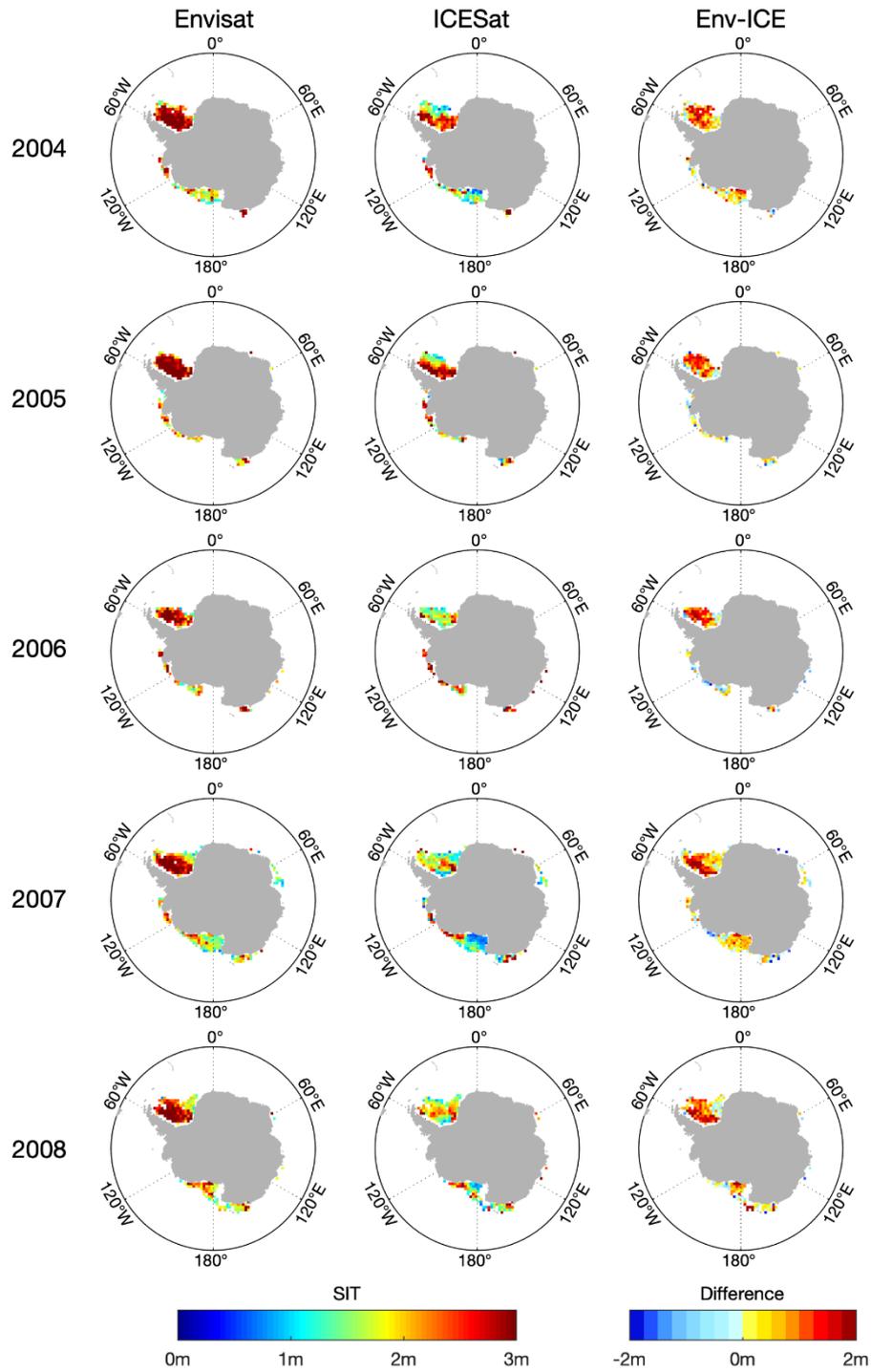
Figure 5: Same as Fig. 4 but for summer (February & March).
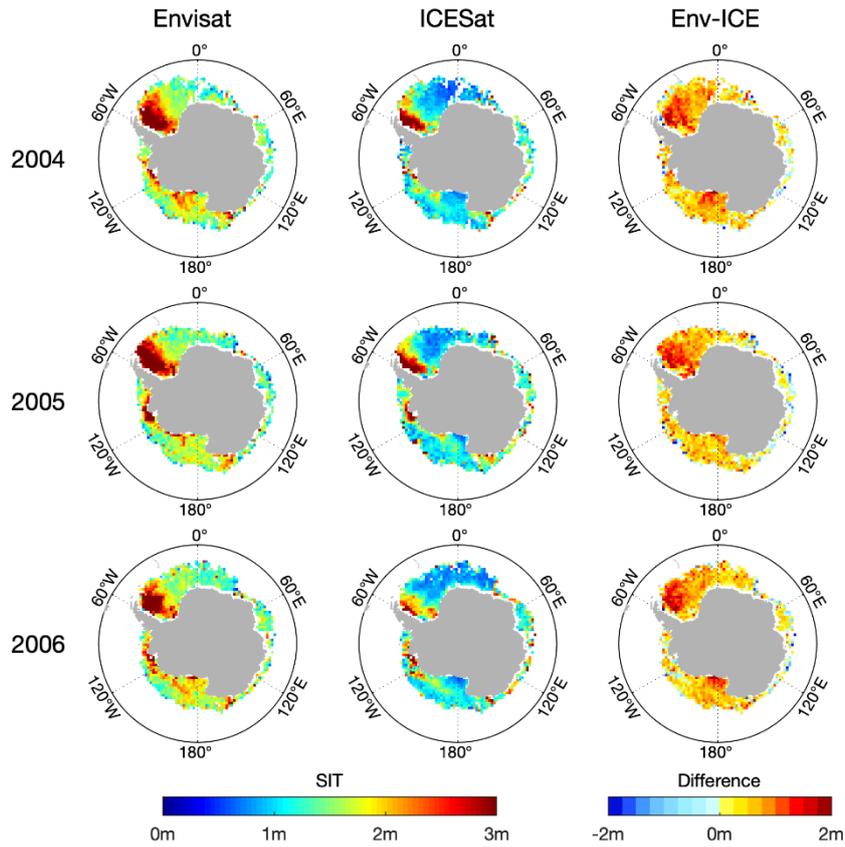
Figure 6: Same as Fig. 4 but for autumn (May & June).
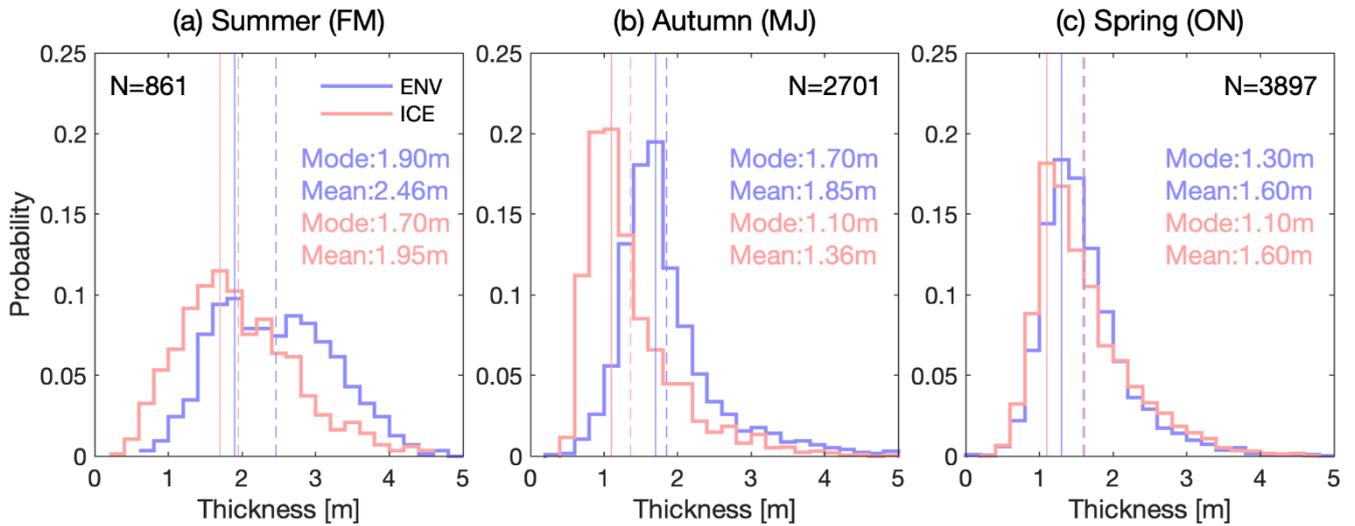
Figure 7: Probability of the Envisat SIT and the ICESat SIT for all the individual comparison pairs. The blue stairs represent Envisat ice thickness and the red stairs represent ICESat ice thickness. The solid lines indicate the modal ice thickness and the dashed lines indicate the mean ice thickness of both data sets. The bin size is 0.2 m and the probability distribution is normalized.
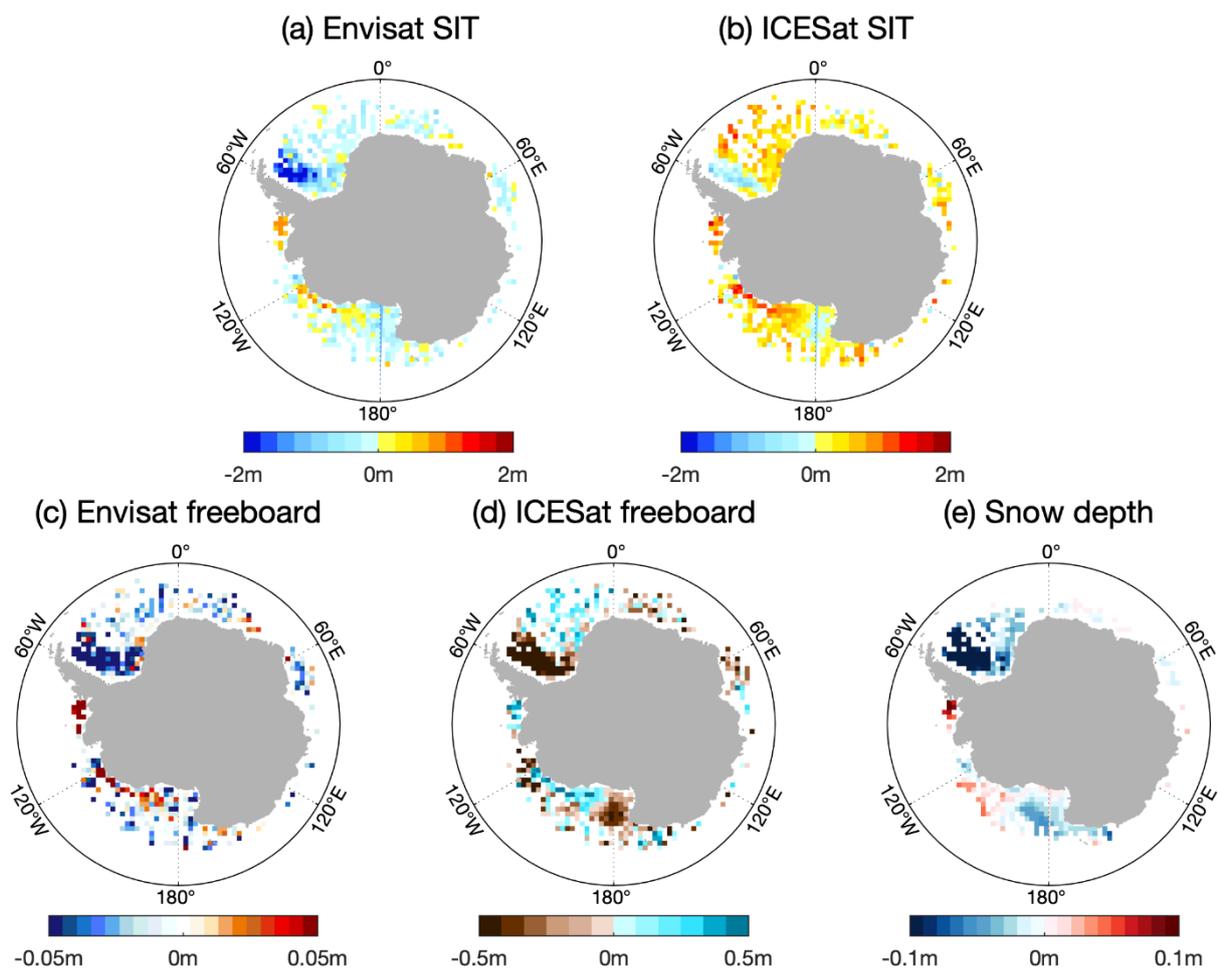
680 **Figure 8:** The average changes of Envisat SIT, ICESat SIT, Envisat freeboard, ICESat freeboard and snow depth climatology used in Envisat retrieval from autumn to spring (MJON) calculated from 2004, 2005 and 2006.
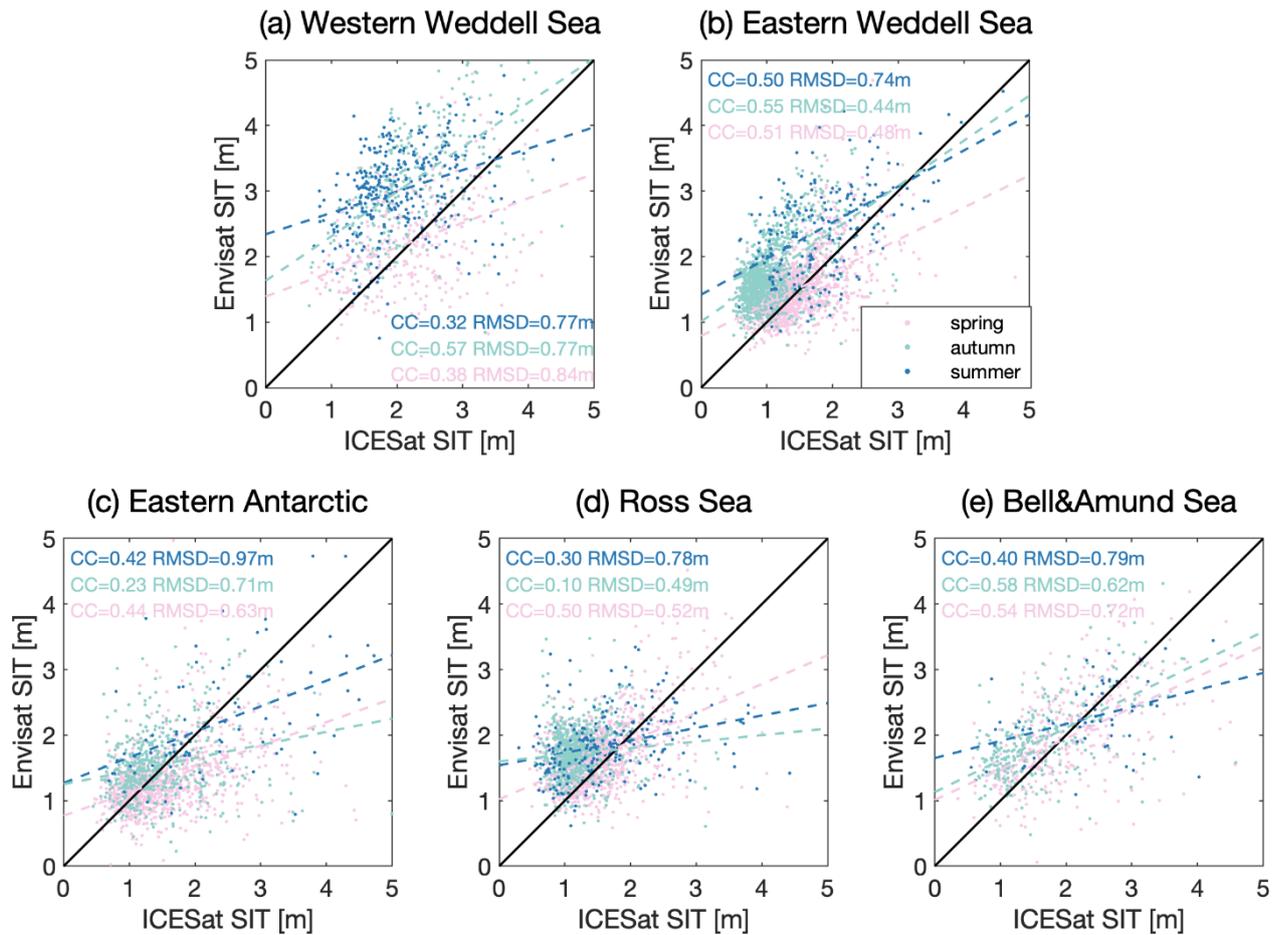
Figure 9: Scatterplots of the individual data pairs between Envisat SIT and ICESat SIT for each region and each season. The data are taken from all seasons available. Since the comparison pairs are too few in Indian Ocean and western Pacific Ocean, we combine these two regions into Eastern Antarctic. The respective correlation coefficients and RMSDs are indicated in the panels. The black line is the 1-to-1 fit line and the dashed colored lines stand for linear regression lines.

685
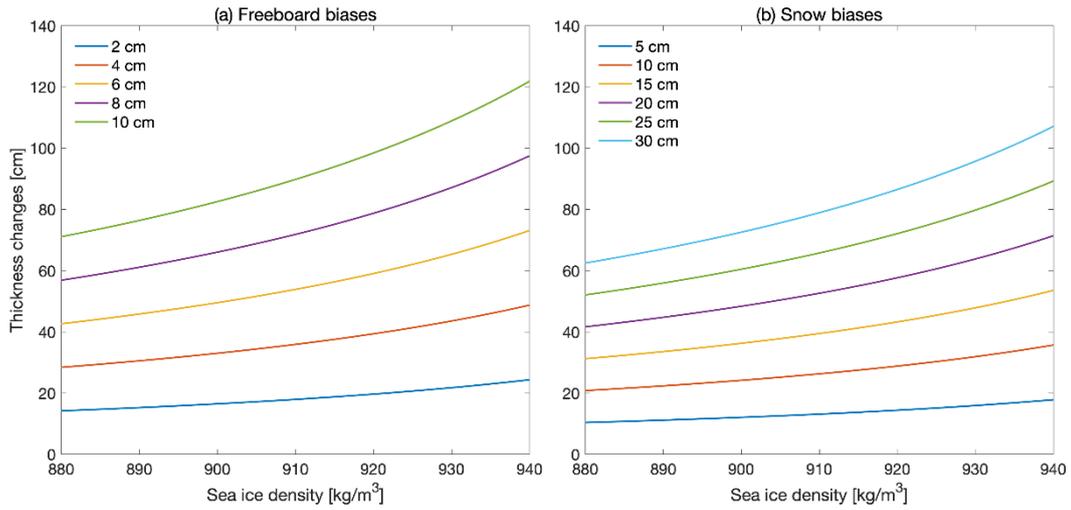
Figure 10: Sensitivity of sea ice thickness changes to sea ice freeboard biases and snow depth biases as function of sea ice density. (a) SIT changes computed with Eq. (1) for different sea ice freeboard biases (2 cm to 10 cm). (b) Similar to (a) but computed for different snow depth biases (5 cm to 30 cm).

Table 1: ICESat operating periods and Envisat periods used for the comparisons. The three seasons are divided according to the ICESat operating periods. Note that ON is Oct-Nov, FM is Feb-Mar, and MJ is May-June.

Years	Summer (FM)		Autumn (MJ)		Spring (ON)	
	ICESat	Envisat	ICESat	Envisat	ICESat	Envisat
2004	Feb 17 to Mar 20	Feb 1 to Mar 31	May 18 to Jun 20	May 1 to Jun 30	Oct 3 to Nov 8	Oct 1 to Nov 31
2005	Feb 17 to Mar 22	Feb 1 to Mar 31	May 20 to Jun 22	May 1 to Jun 30	Oct 21 to Nov 23	Oct 1 to Nov 31
2006	Feb 22 to Mar 26	Feb 1 to Mar 31	May 24 to Jun 25	May 1 to Jun 30	Oct 25 to Nov 26	Oct 1 to Nov 31
2007	Mar 12 to Apr 14	Mar 1 to Apr 30	–	–	Oct 2 to Nov 4	Oct 1 to Nov 31
2008	Feb 17 to Mar 20	Feb 1 to Mar 31	–	–	–	–

Table 2: A summary of the sea ice thickness data used during the comparison, including different data sources, spatial resolution, temporal resolution and snow product.

Source	Instrument	Operation time	Footprint	Grid resolution	Temporal resolution	Snow product
Envisat satellite	Radar altimeter	2002-2011	2–10 km	50 km grid	Monthly average	AMSR-E climatology
ICESat satellite	Laser altimeter	2003-2009	70 m	100 km grid	See Table 1	ASPeCt observations
Weddell Sea ULS	Upward Looking Sonars	1990-2010	6–8 m	Single point	Monthly average	built into Eq. (4)

700

Table 3: Respective operation times of the ULS, Envisat and ICESat sea ice thickness data set during the comparison between ULS and satellite SIT.

	ULS	ENV	ICE
Site 207	Apr 2005 to Mar 2008	Apr 2005 to Mar 2008	MJ05 to FM08
Site 229	Jan 2003 to Nov 2005	Jan 2003 to Nov 2005	FM04 to ON05
Site 231	Mar 2005 to Feb 2008	Mar 2005 to Feb 2008	FM05 to ON07

Table 4: Statistical results of the comparison between two satellite SIT data with ULS data. N is the number of comparison pairs.

Site	Env-ULS			ICE-ULS			N
	MD (m)	SD (m)	RMSD (m)	MD (m)	SD (m)	RMSD (m)	

207	1.63	0.67	0.60	1.73	0.70	0.62	5
229	0.72	0.61	0.43	0.42	0.07	0.05	2
231	1.11	0.41	0.33	0.55	0.29	0.24	3
Average	1.29	0.65	0.62	1.11	0.81	0.77	10

Table 5: Statistical results of the comparisons between Envisat sea ice thickness and ICESat sea ice thickness for each ICESat operating period. The correlation coefficients (CC) in italic type have not passed the 95% significance test. N is the number of comparison pairs.

		ENV(SD) (m)	ICE(SD) (m)	Difference (SD) (m)	RMSD (m)	CC	N
Summer (FM)	Seasonal average	2.51(0.66)	1.99(0.58)	0.52(0.68)	0.68	0.40	170
	2004	2.56(0.76)	2.00(0.79)	0.56(0.77)	0.77	0.51	179
	2005	2.82(0.82)	2.35(0.82)	0.47(0.85)	0.84	0.47	139
	2006	2.47(0.69)	2.07(0.74)	0.40(1.02)	1.02	*0.00*	122
	2007	2.16(0.76)	1.69(0.80)	0.47(0.88)	0.88	0.36	236
	2008	2.45(0.82)	1.87(0.61)	0.58(0.92)	0.91	*0.21*	185
Autumn (MJ)	Seasonal average	1.92(0.65)	1.35(0.55)	0.57(0.45)	0.47	0.71	735
	2004	1.87(0.70)	1.33(0.62)	0.54(0.58)	0.58	0.61	887
	2005	1.88(0.76)	1.42(0.68)	0.46(0.66)	0.66	0.58	903
	2006	1.81(0.61)	1.32(0.58)	0.49(0.62)	0.62	0.46	911
Spring (ON)	Seasonal average	1.62(0.48)	1.62(0.50)	0.00(0.39)	0.39	0.68	886
	2004	1.63(0.60)	1.65(0.67)	-0.02(0.60)	0.60	0.57	1057

		ENV(SD) (m)	ICE(SD) (m)	Difference(SD) (m)	RMSD (m)	CC	N
	2005	1.59(0.60)	1.53(0.65)	0.06(0.62)	0.62	0.51	888
	2006	1.48(0.54)	1.64(0.66)	-0.16(0.58)	0.58	0.55	828
	2007	1.67(0.59)	1.57(0.59)	0.10(0.58)	0.58	0.52	1124

705

Table 6: Statistical results of the comparisons between Envisat sea ice thickness and ICESat sea ice thickness for each region divided as Fig. 9. N is the numbers of comparison pairs, taking into account the actual number of values per season.

		ENV(SD) (m)	ICE(SD) (m)	Difference(SD) (m)	RMSD (m)	CC	N
W. Weddell	Regional average	2.80(0.87)	2.17(0.72)	0.63(0.91)	0.91	0.36	892
	summer (FM)	3.01(0.67)	2.04(0.66)	0.97(0.77)	0.77	0.32	329
	autumn (MJ)	3.18(0.88)	2.28(0.74)	0.90(0.77)	0.77	0.57	263
	spring (ON)	2.23(0.75)	2.23(0.76)	0.00(0.84)	0.84	0.38	300
E. Weddell	Regional average	1.69(0.59)	1.35(0.54)	0.34(0.58)	0.58	0.46	2405
	summer (FM)	2.45(0.77)	1.87(0.70)	0.58(0.74)	0.74	0.50	210
	autumn (MJ)	1.76(0.51)	1.08(0.40)	0.68(0.45)	0.44	0.55	921
	spring (ON)	1.51(0.48)	1.46(0.49)	0.05(0.48)	0.48	0.51	1274
Eastern Antarctic	Regional average	1.45(0.59)	1.57(0.69)	-0.12(0.69)	0.69	0.42	1535
	summer (FM)	2.20(0.84)	2.36(1.05)	-0.16(0.98)	0.97	0.49	81
	autumn (MJ)	1.55(0.53)	1.49(0.61)	0.06(0.71)	0.71	0.23	521
	spring (ON)	1.32(0.52)	1.55(0.65)	-0.23(0.63)	0.63	0.44	933
Ross Sea	Regional average	1.72(0.45)	1.41(0.55)	0.31(0.57)	0.57	0.36	2047

	summer (FM)	1.85(0.49)	1.64(0.77)	0.21(0.78)	0.78	0.30	215
	autumn (MJ)	1.72(0.37)	1.20(0.37)	0.53(0.49)	0.49	0.10	749
	spring (ON)	1.69(0.49)	1.52(0.55)	0.17(0.52)	0.52	0.50	1083
Bell/Amund	Regional average	1.96(0.65)	1.87(0.80)	0.09(0.71)	0.71	0.54	694
	summer (FM)	2.26(0.54)	2.31(0.82)	-0.05(0.79)	0.79	0.40	63
	autumn (MJ)	1.92(0.60)	1.62(0.72)	0.30(0.62)	0.62	0.58	282
	spring (ON)	1.95(0.69)	2.00(0.79)	-0.05(0.72)	0.72	0.54	349